Research Paper

GEOSPHERE

GEOSPHERE, v. 16, no. 4

https://doi.org/10.1130/GES02094.1

12 figures; 1 table in 2 parts; 1 set of supplemental files

CORRESPONDENCE: cjbusby@ucdavis.edu

CITATION: Busby, C., Graettinger, A., López Martínez, M., Medynski, S., Niemi, T., Andrews, C., Bowman, E., Gutierrez, E.P., Henry, M., Lodes, E., Ojeda, J., Rice, J., Andrews, G., and Brown, S., 2020, Volcanic record of the arc-to-rift transition onshore of the Guaymas basin in the Santa Rosalía area, Gulf of California, Baja California: Geosphere, v. 16, no. 4, p. 1723–1752, https://doi.org/10.1130/GES02094.1.

Science Editor: Shanaka de Silva

Received 27 November 2018
Revision received 27 December 2019
Accepted 21 February 2020

Published online 26 May 2020

Volcanic record of the arc-to-rift transition onshore of the Guaymas basin in the Santa Rosalía area, Gulf of California, Baja California

Cathy Busby[1], Alison Graettinger[2], Margarita López Martínez[3], Sarah Medynski[1], Tina Niemi[2], Claire Andrews[4], Emilie Bowman[4], Evelyn P. Gutierrez[5], Matthew Henry[2], Emma Lodes[6], Judith Ojeda[7], Jonathan Rice[8], Graham Andrews[9], and Sarah Brown[10]

[1]Department of Earth and Planetary Sciences, University of California, Davis, 2119 Earth and Physical Sciences, One Shields Avenue, Davis, California 95616, USA
[2]Department of Geosciences, University of Missouri–Kansas City, 5100 Rockhill Road, Kansas City, Missouri, USA
[3]Depto. Geología, Centro de Investigación Científica y de Educación Superior de Ensenada, Baja California, México
[4]Jackson School of Geosciences, University of Texas at Austin, Austin, Texas 78759, USA
[5]Department of Geological Sciences, California State University, 800 N. State College Boulevard, Fullerton, California 91832, USA
[6]Department of Geology, Occidental College, Los Angeles, California 90041, USA
[7]Departamento de Ingenieria en Minas Metalurgia y Geología, Universidad de Guanajuato, Guanajuato, 36000, Mexico
[8]Department of Geological Sciences, San Diego State University, San Diego, California 92182, USA
[9]Department of Geology and Geography, Brooks Hall, West Virginia University, 93 Beechurst Avenue, Morgantown, West Virginia 26506, USA
[10]West Virginia Geological and Economic Survey, 1 Mont Chateau Road, Morgantown, West Virginia 26508, USA

ABSTRACT

The Gulf of California is an archetype of continental rupture through transtensional rifting, and exploitation of a thermally weakened arc to produce a rift. Volcanic rocks of central Baja California record the transition from calcalkaline arc magmatism, due to subduction of the Farallon plate (ca. 24–12 Ma), to rift magmatism, related to the opening of the Gulf of California (<12 Ma). In addition, a suite of postsubduction rocks (<12 Ma), referred to as "bajaites," are enriched in light rare-earth and other incompatible elements (e.g., Ba and Sr). These are further subdivided into high-magnesian andesite (with 50%–58% SiO_2 and MgO >4%) and adakite (>56% SiO_2 and MgO <3%). The bajaites correlate spatially with a fossil slab imaged under central Baja and are inferred to record postsubduction melting of the slab and subduction-modified mantle by asthenospheric upwelling associated with rifting or slab breakoff. We report on volcanic rocks of all three suites, which surround and underlie the Santa Rosalía sedimentary rift basin. This area represents the western margin of the Guaymas basin, the most magmatically robust segment of the Gulf of California rift, where seafloor spreading occurred in isolation for 3–4 m.y. (starting at 6 Ma) before transtensional pull-apart basins to the north and south ruptured the continental crust. Outcrops of the Santa Rosalía area thus offer the opportunity to understand the magmatic evolution of the Guaymas rift, which has been the focus of numerous oceanographic expeditions.

We describe 21 distinct volcanic and hypabyssal map units in the Santa Rosalía area, using field characteristics, petrographic data, and major- and trace-element geochemical data, as well as zircon isotopic data and ten new ^{40}Ar-^{39}Ar ages. Lithofacies include lavas and lava domes, block-and-ash-flow tuffs, ignimbrites, and hypabyssal intrusions (plugs, dikes, and peperites). Calcalkaline volcanic rocks (13.81–10.11 Ma) pass conformably upsection, with no time gap, into volcanic rocks with rift transitional chemistry (9.69–8.84 Ma). The onset of rifting was marked by explosive eruption of silicic ignimbrite (tuff of El Morro), possibly from a caldera, similar to the onset of rifting or accelerated rifting in other parts of the Gulf of California. Epsilon Hf zircon data are consistent with a rift transitional setting for the tuff of El Morro. Arc and rift volcanic rocks were then juxtaposed by normal faults and tilted eastward toward a north-south fault that lay offshore, likely related to the north-south normal faults documented for the early history of the Guaymas basin, prior to the onset of northwest-southeast transtenional faulting. Magmatism in the Santa Rosalía area resumed with emplacement of high-magnesian andesite lavas and intrusions, at 6.06 Ma ± 0.27 Ma, coeval with the onset of seafloor spreading in the Guaymas basin at ca. 6 Ma.

The 9.69–8.84 Ma rift transitional volcanic rocks underlying the Santa Rosalía sedimentary basin provide a maximum age on its basal fill. Evaporites in the Santa Rosalía sedimentary basin formed on the margin of the Guaymas basin, where thicker evaporites formed. Overlying coarse-grained clastic sedimentary fill of the Santa Rosalía basin and its stratiform Cu-Co-Zn-Mn sulfides may have accumulated rapidly, coeval with emplacement of 6.06 Ma high-magnesian andesite intrusions and the ca. 6 Ma onset of seafloor spreading in the Guaymas basin.

INTRODUCTION

Previous work established that volcanic rocks of the Santa Rosalía area (Fig. 1) record an arc-rift transition, from subduction of the Farallon plate, to rift magmatism related to the opening of the Gulf of California (Conly et al., 2005). Subduction and rifting in the Gulf of California region are estimated to be ca. 24–12 Ma and ca. 12 Ma to present, respectively, using plate tectonic models (e.g., Atwater, 1970; Gastil et al., 1979; Atwater, 1989; Stock and Hodges, 1989, 1990; Lonsdale, 1991; Atwater and Stock, 1998; Henry and Aranda-Gomez, 2000; Michaud et al., 2006; Umhoefer, 2011). Furthermore, the geochemistry of volcanic rocks of the Gulf of California region is generally consistent with a change from subduction (referred to as Comondú Group, Fig. 1) to rifting at ca. 12 Ma (e.g., Hausback, 1984; Sawlan and Smith, 1984; Sawlan, 1991;

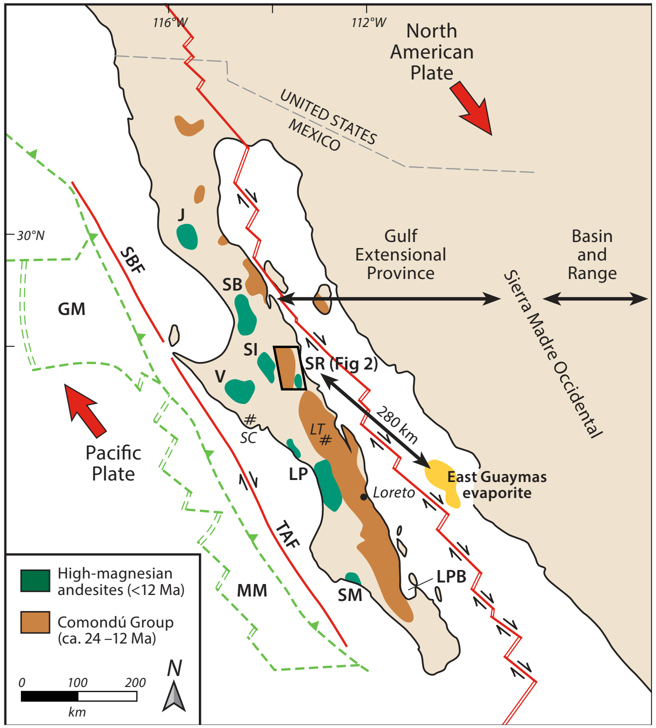

Figure 1. Simplified map of Cenozoic volcanic rocks of the Baja California Peninsula and seafloor structures in the Gulf of California and Pacific margins to the east and west, respectively (data from Hausback, 1984; McLean et al., 1987; Lizarralde et al., 2007; Calmus et al., 2011; Miller and Lizarralde, 2013; Di Luccio et al., 2014; Darin et al., 2016; Drake et al., 2017; Ferrari et al., 2018). Comondú Group subduction-related volcanic rocks in the Santa Rosalía area (SR) include rift transitional rocks described herein and perhaps in other areas not yet discovered. The Santa Rosalía area lies within the Gulf Extensional Province, which in turn is partly separated from the Basin and Range by unextended Cenozoic volcanic rocks in the core of the Sierra Madre Occidental of mainland Mexico (Cenozoic volcanic rocks on mainland not shown here). The East Guaymas evaporite has been displaced 280 km from its position adjacent to evaporites at Santa Rosalía (Miller and Lizarralde, 2013); the Santa Rosalía evaporites are shown on Figure 12. Volcanic fields with high-magnesian andesites include: J—Jaraguay; SB—San Borja; SI—San Ignacio; V—Vizcaino; LP—La Purisma; and SM—Santa Margarita. Geographic features discussed in text: SR—Santa Rosalía; and LPB—La Paz Bay (see references in text). Geologic features: GM—Guadalupe microplate; MM—Magdalena microplate; TAF—Tosco-Abreojos fault; and SBF—San Benito fault. Adakites described in text include Santa Clara volcanic field (#SC) and La Trinidad (#LT). Red single line indicates active fault, and red double line indicates active spreading center. Green dashed lines indicate inactive spreading centers, transforms, and trench. Large red arrows indicate motion between Pacific plate and North American plate. Capture of the Baja California microplate by the Pacific plate is essentially complete with ~90% of Pacific–North American plate motion now accommodated by the Gulf of California (Michaud et al., 2004) and oceanic spreading centers established along the entire length of the rift (Schmitt et al., 2013).

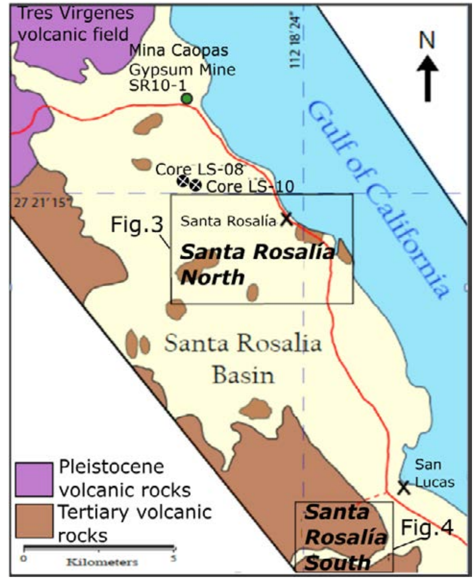

Figure 2. Miocene to Pliocene sedimentary rocks of the Santa Rosalía basin (shown in yellow) are underlain by Tertiary volcanic rocks (described herein) and overlain by Pleistocene volcanic rocks (Schmitt et al., 2006, 2010). Positions of cores and outcrop localities (SR10-1) outside of detailed map areas are plotted here (Table 1A).

Martín-Barajas et al., 1995, 2000; Paz Moreno and Demant, 1999; Ferrari et al., 2005), although residual arc signatures persisted for 4 m.y. in Sonora (Till et al., 2009) and recurred in the Quaternary at Tres Virgenes volcanic field (Fig. 2; Sawlan, 1991; Schmitt et al., 2006, 2010). The Gulf of California ruptured much more rapidly than is typical of continental rifts, at least partly because it exploited the thermally weakened Comondú arc axis (Umhoefer, 2011), but also because pull-apart basins are the most efficient tectonic setting for localizing rapid thinning of the crust (Christie-Blick and Biddle, 1985; Nilsen and McLaughlin, 1985; Pitman and Andrews, 1985; Nilsen and Sylvester, 1995; Xie and Heller, 2009; Umhoefer, 2011; Allen and Allen, 2013). In this paper, we explore in detail the geology of the arc-rift transition, preserved in the Santa Rosalía area (Figs. 2–4).

The Santa Rosalía area also offers insight into the processes that produced the Guaymas basin (Fig. 1). This basin has been the focus of two Deep Sea Drilling Project and Integrated Ocean Drilling Program (DSDP/IODP) expeditions, as well as wide-angle and multi-channel seismic surveys (Curray et al., 1982; Lizarralde et al., 2007; Miller and Lizarralde, 2013; Teske et al., 2018). Tectonic reconstructions show that the 2-km-thick evaporite body imaged by multi-channel seismic surveys in the Guaymas basin was fringed by thinner (up to ~70-m-thick) gypsum deposits exposed onshore in the Santa Rosalía basin (Fig. 1; Miller and Lizarralde, 2013). However, the evaporite and underlying crustal rocks in the Guayamas basin have not been sampled or dated. The Santa Rosalía area offers the opportunity to do this.

Seafloor spreading in the Gulf of California initiated in the Guaymas basin at ca. 6 Ma, and occurred in isolation for 3–4 m.y. before transtensional pull-apart basins to the north and south

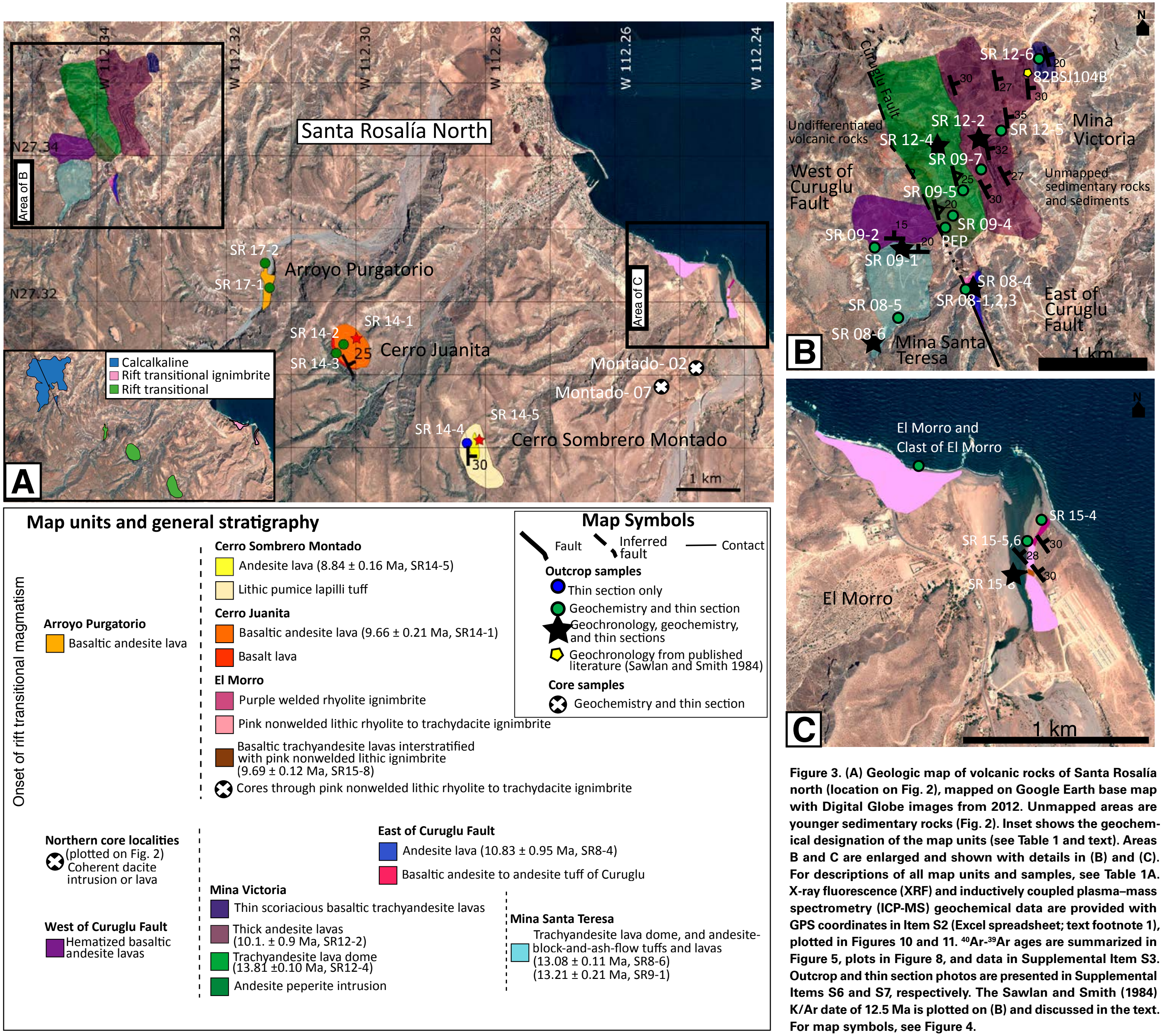

Figure 3. (A) Geologic map of volcanic rocks of Santa Rosalía north (location on Fig. 2), mapped on Google Earth base map with Digital Globe images from 2012. Unmapped areas are younger sedimentary rocks (Fig. 2). Inset shows the geochemical designation of the map units (see Table 1 and text). Areas B and C are enlarged and shown with details in (B) and (C). For descriptions of all map units and samples, see Table 1A. X-ray fluorescence (XRF) and inductively coupled plasma–mass spectrometry (ICP-MS) geochemical data are provided with GPS coordinates in Item S2 (Excel spreadsheet; text footnote 1), plotted in Figures 10 and 11. ^{40}Ar-^{39}Ar ages are summarized in Figure 5, plots in Figure 8, and data in Supplemental Item S3. Outcrop and thin section photos are presented in Supplemental Items S6 and S7, respectively. The Sawlan and Smith (1984) K/Ar date of 12.5 Ma is plotted on (B) and discussed in the text. For map symbols, see Figure 4.

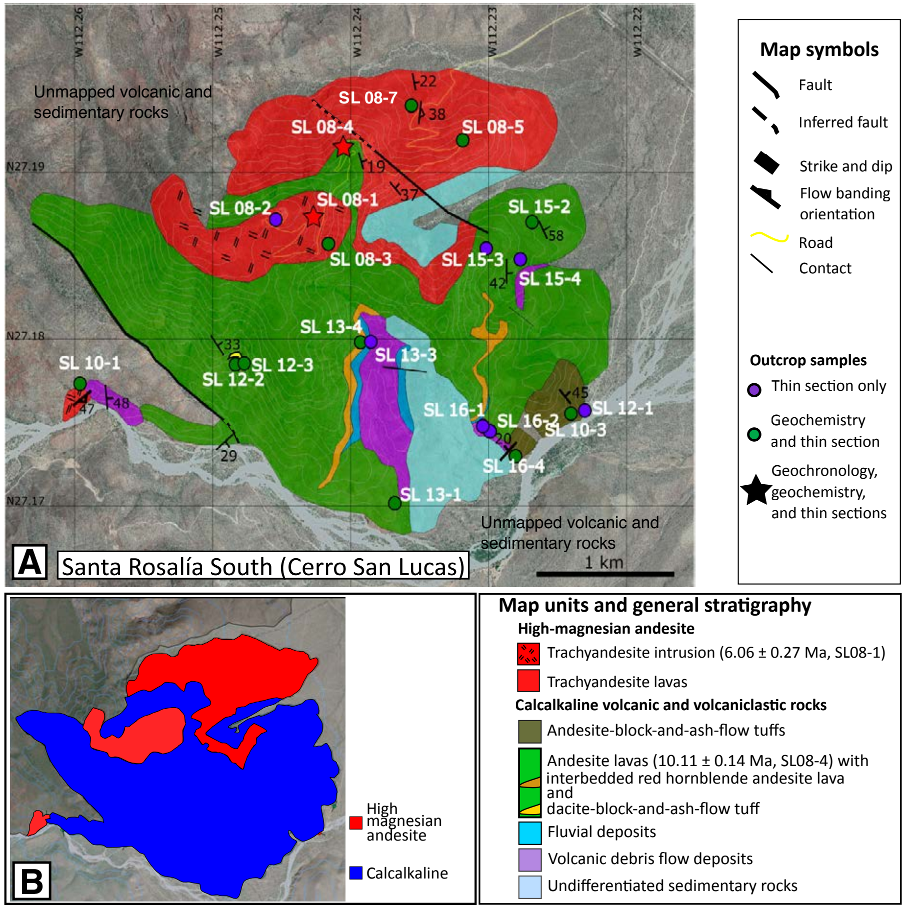

Figure 4. (A) Geologic map of volcanic rocks of Santa Rosalía south (Cerro San Lucas, location on Fig. 2), mapped on Google Earth base map with Digital Globe imagery from 2018, WGS 1984. ASTER GDEM V2.0 30 m contours courtesy of Ministry of Economy, Trade, and Industry (METI) and National Aeronautics and Space Administration (NASA). Map units are described in Table 1B. Geochemical and geochronological data, and outcrop and thin section photos, are called out in Figure 3. High-magnesian andesite is distinguished using criteria given in Supplemental Item S6 (text footnote 1). (B) Geochemical designation of the map units (see Table 1 and text).

ruptured the continental crust (Lizarralde et al., 2007; Sutherland et al., 2012; Martín-Barajas et al., 2013; Umhoefer et al., 2018). Guaymas basin is also a more magma-rich rift than the other segments (Lizarralde et al., 2007). Why did this segment succeed first, in the center of a seaway that extended ~700 km to the north and ~750 km to the south? Lizarralde et al. (2007) attempted to address this question but arrived at no clear resolution. We show here that high-magnesian andesite magmatism in the Santa Rosalía area was coeval with the onset of seafloor spreading in the Guaymas basin at 6 Ma. The distribution of high-magnesian andesites (shown on Fig. 1) correlates spatially with remnant slabs geophysically imaged under central Baja California. These andesites have generally been regarded as the product of postsubduction slab-window magmatism (Benoit et al., 2002; Calmus et al., 2003; Bellon et al., 2006; Pallares et al., 2007, 2008; Castillo, 2008; Negrete-Aranda and Cañón-Tapia, 2008; Negrete-Aranda et al., 2010, 2013; Calmus et al., 2011; Di Luccio et al., 2014). The high-magnesian andesites in the Santa Rosalía area lie far inboard from the paleotrench, relative to other high-magnesian andesites in central Baja California (Fig. 1). We discuss the possibility that this was controlled by a slab tear that crosses beneath the Baja California Peninsula between the Guadalupe and Magdalena plates. This tear was imaged by Di Luccio et al. (2014) as a low-velocity (hot) zone, and we discuss how this tear may have promoted early rupture and magma-rich seafloor spreading in the Guaymas basin.

Much attention has also been focused on the origin and age of Cu-Zn-Co-Mn stratiform deposits of the Boleo Formation sedimentary rift basin fill at Santa Rosalía (Wilson and Rocha, 1955; Schmidt, 1975; Holt et al., 2000; Ochoa-Landín et al., 2000; Conly et al., 2006, 2011). These deposits have been mined for more than a century and are currently the target of a multibillion-dollar mining operation, the Minera Boleo. Although these ore beds lie within clastic sedimentary rocks that rest upon and interfinger with the evaporates described above, their age is poorly constrained. We present arguments for the interpretation that the ore beds formed rapidly, during emplacement of slab window high-magnesian andesite intrusions and onset of Guaymas basin seafloor spreading at 6 Ma.

REGIONAL SETTING

Regional-scale tectonic reconstructions have delineated four main phases in the evolution of the Gulf of California (Gastil et al., 1979; Angelier et al., 1981; Atwater, 1989; Stock and Hodges, 1989, 1990; Lonsdale, 1991; Axen, 1995; Axen and Fletcher, 1998; Henry and Aranda-Gomez, 2000; Martín-Barajas et al., 2000; Stock, 2000; Oskin et al., 2001; Oskin and Stock, 2003a, 2003b, 2003c; Michaud et al., 2006; Lizarralde et al., 2007; Umhoefer, 2011; Sutherland et al., 2012; Duque-Trujillo et al., 2015; Darin et al., 2016; Drake et al., 2017):

(1) Forearc volcaniclastic sedimentation in what is now the Gulf of California (ca. 28–19 Ma), between a subduction zone to the west and an extensional continental arc to the east that produced large-volume explosive caldera-forming silicic eruptions due to slab rollback (Sierra Madre Occidental). Distal and reworked equivalents of these ignimbrites were deposited in the forearc region, in what is now the Gulf of California region.

(2) Continued slab rollback caused westward sweep of the volcanic arc into what is now the Gulf of California region, referred to as the Comondú Group or Comondú arc (ca. 19–12 Ma), at least locally accompanied by E-W extension, both over a narrow (~100 km) region. This sweep was generally accompanied by a shift to effusive volcanism with intermediate compositions. These rocks now form the main peninsular escarpment in Baja California (Sawlan and Smith, 1984).

(3) End of subduction and onset of continental rift and/or slab window volcanism in what is now the Gulf of California region. The relative importance of E-W extension and NW-SE transtension remains controversial for this time frame (ca. 12–6 Ma). Volcanic rocks of this age include basalts and the products of large-volume silicic explosive eruptions (ignimbrites). As subduction volcanism waned, the "bajaites" described above were erupted across central Baja California.

(4) Continental separation and onset of seafloor spreading, under a NW-SE transtensional regime with ongoing continental rift and slab window volcanism (ca. 8–6 Ma to present).

The Gulf of California is an outstanding place to study the geologic processes described above, because exposures are superb, and the young volcanic rocks that record these processes are relatively unaltered. For this reason, volcanic rocks have been studied along many parts of the Gulf of California (e.g., Hausback, 1984; Sawlan and Smith, 1984; McLean et al., 1987; Stock and Hodges, 1989; Sawlan, 1991; Martín-Barajas et al., 1995, 1997; Paz Moreno and Demant, 1999; Delgado Argote et al., 2000; Stock, 2000; Umhoefer et al., 2001; Escalona Alcazar et al., 2001; Ferrari et al., 2005; Schmitt et al., 2010; Bennett et al., 2013; Ferrari et al., 2013; Bennett et al., 2015; García-Sánchez et al., 2016; Osorio-Ocampo et al., 2016; Ferrari et al., 2018). However, only one paper has focused on magmatism in the Santa Rosalía area (Conly et al., 2005). This represents a gap in knowledge of the timing and nature of magmatism on the margin of the well-studied, magmatically robust Guaymas rift.

ANALYTICAL METHODS

Analytical methods are detailed in Supplemental Item 1[1], hereafter referred to as Item S1. These include X-ray fluorescence (XRF) and inductively coupled plasma–mass spectrometry (ICP-MS) whole-rock geochemical analysis methods, ^{40}Ar-^{39}Ar geochronologic methods, and methods for obtaining U-Pb and Hf isotopic analyses on zircons. Analytical data are given in Item S3 (footnote 1) for ^{40}Ar-^{39}Ar, Item S4 for U-Pb zircons, and Item S5 for Hf isotopes in zircon.

For the first time in the Santa Rosalía area (Figs. 1 and 2), we present detailed volcanic lithofacies maps (Figs. 3 and 4), volcanic stratigraphy (Fig. 5 and Table 1), outcrop photos (Fig. 6 and Item S6), and photomicrographs (Fig. 7 and Item S7), as well as geochemical data on samples located by GPS (Item S2), with samples plotted on the maps (Figs. 3 and 4).

MAPPING METHODS

Our mapping has focused on two main areas (Fig. 2), Santa Rosalía north (Fig. 3 and Table 1A) and Santa Rosalía south (Fig. 4 and Table 1B), separated by sedimentary rocks of the overlying Santa Rosalía basin. The Santa Rosalía north geologic map (Fig. 2) was mapped on Google Earth base map with Digital Globe images from 2012. The

Geochemical designation	Area, map unit name	Sample name	^{40}Ar/^{39}Ar Age in Ma		Sample #
High-magnesian Andesite	Santa Rosalía south, high- magnesian trachyandesite intrusion	Cpx hb high-magnesian trachyandesite hypabyssal intrusion	Hb	6.06 ± 0.27	SL 08-1
Rift Transitional Lavas	Cerro Sombrero Montado, andesite lava	Phenocryst-poor andesite lava	WR	8.84 ± 0.16	SR 14-5
	Cerro Juanita, basaltic andesite lava	Phenocryst-poor basaltic andesite lava	WR	9.66 ± 0.21	SR 14-1
Rift transitional ignimbrites	El Morro, basaltic trachyandesite lavas interstratified with pink non-welded lithic ignimbrite	Basaltic trachyandesite lava	GM	9.69 ± 0.12	SR 15-8
Calcalkaline	Santa Rosalía South, andesite lava	Crystal-rich cpx andesite lava	GM	10.11 ± 0.14	SL 08-4
	East of Curuglu fault, andesite lava	Hb cpx andesite lava	GM	10.83 ± 0.95	SR 08-4
	Mina Victoria, thick andesite lavas	Hb cpx andesite lava	GM	10.1 ± 0.9	SR 12-2
	Mina Santa Teresa, trachyandesite lava dome and andesite block-and-ash-flow tuffs and lavas	Hb cpx trachyandesite lava dome interior	GM	13.08 ± 0.11	SR 08-6
	Mina Santa Teresa, trachyandesite lava dome, and andesite block-and-ash-flow tuffs and lavas	Hb cpx andesite lava	GM	13.21 ± 0.21	SR 09-1
	Mina Victoria, trachyandesite lava dome	Hb cpx trachyandesite lava dome interior	GM	13.81 ± 0.10	SR 12-4

Figure 5. Summary of volcanic and intrusive units rocks dated by ^{40}Ar-^{39}Ar, grouped by geochemical designation (calcalkaline, rift transitional ignimbrites, rift transitional lavas, and high-magnesian andesites), discussed in text. ^{40}Ar-^{39}Ar plots shown in Figure 8, with data and methods given in Supplemental Item S2 (text footnote 1). Area and map unit names match the map keys (Figs. 3 and 4) and Table 1. Age sample numbers are plotted on maps (Figs. 3 and 4), and GPS coordinates are given in Item S1. Material dated: Cpx—clinopyroxene; Hb—hornblende; WR—whole rock; and GM—groundmass.

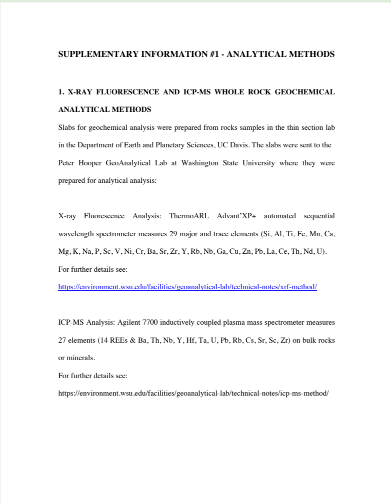
SUPPLEMENTARY INFORMATION #1 - ANALYTICAL METHODS

1. X-RAY FLUORESCENCE AND ICP-MS WHOLE ROCK GEOCHEMICAL ANALYTICAL METHODS

Slabs for geochemical analysis were prepared from rocks samples in the thin section lab in the Department of Earth and Planetary Sciences, UC Davis. The slabs were sent to the Peter Hooper GeoAnalytical Lab at Washington State University where they were prepared for analytical analysis:

X-ray Fluorescence Analysis: ThermoARL Advant'XP+ automated sequential wavelength spectrometer measures 29 major and trace elements (Si, Al, Ti, Fe, Mn, Ca, Mg, K, Na, P, Sc, V, Ni, Cr, Ba, Sr, Zr, Y, Rb, Nb, Ga, Cu, Zn, Pb, La, Ce, Th, Nd, U).
For further details see:
https://environment.wsu.edu/facilities/geoanalytical-lab/technical-notes/xrf-method/

ICP-MS Analysis: Agilent 7700 inductively coupled plasma mass spectrometer measures 27 elements (14 REEs & Ba, Th, Nb, Y, Hf, Ta, U, Pb, Rb, Cs, Sr, Sc, Zr) on bulk rocks or minerals.
For further details see:
https://environment.wsu.edu/facilities/geoanalytical-lab/technical-notes/icp-ms-method/

[1]Supplemental Items. Item S1: Analytical methods, including XRF and ICP-MS whole-rock geochemical analysis, ^{40}Ar-^{39}Ar geochronological analytical methods, and zircon isotopic methods. Item S2: Excel spreadsheet of whole-rock geochemical data, including XRF and LA-ICPMS data. Item S3: ^{40}Ar-^{39}Ar geochronological data: Summary table, and data tables and plots for each sample. Item S4: U-Pb zircon data. Item S5. Hf-isotope zircon data. Item S6: Outcrop photos. Item 7: Photomicrographs, including examples of all samples dated by ^{40}Ar-^{39}Ar. Item S8: Summary of published definitions of adakites and high magnesium andesites. Item S9: KMZ files for geologic maps. Please visit **https://doi.org/10.1130/GEOS.S.12635987** to access the supplemental material, and contact editing@geosociety.org with any questions.

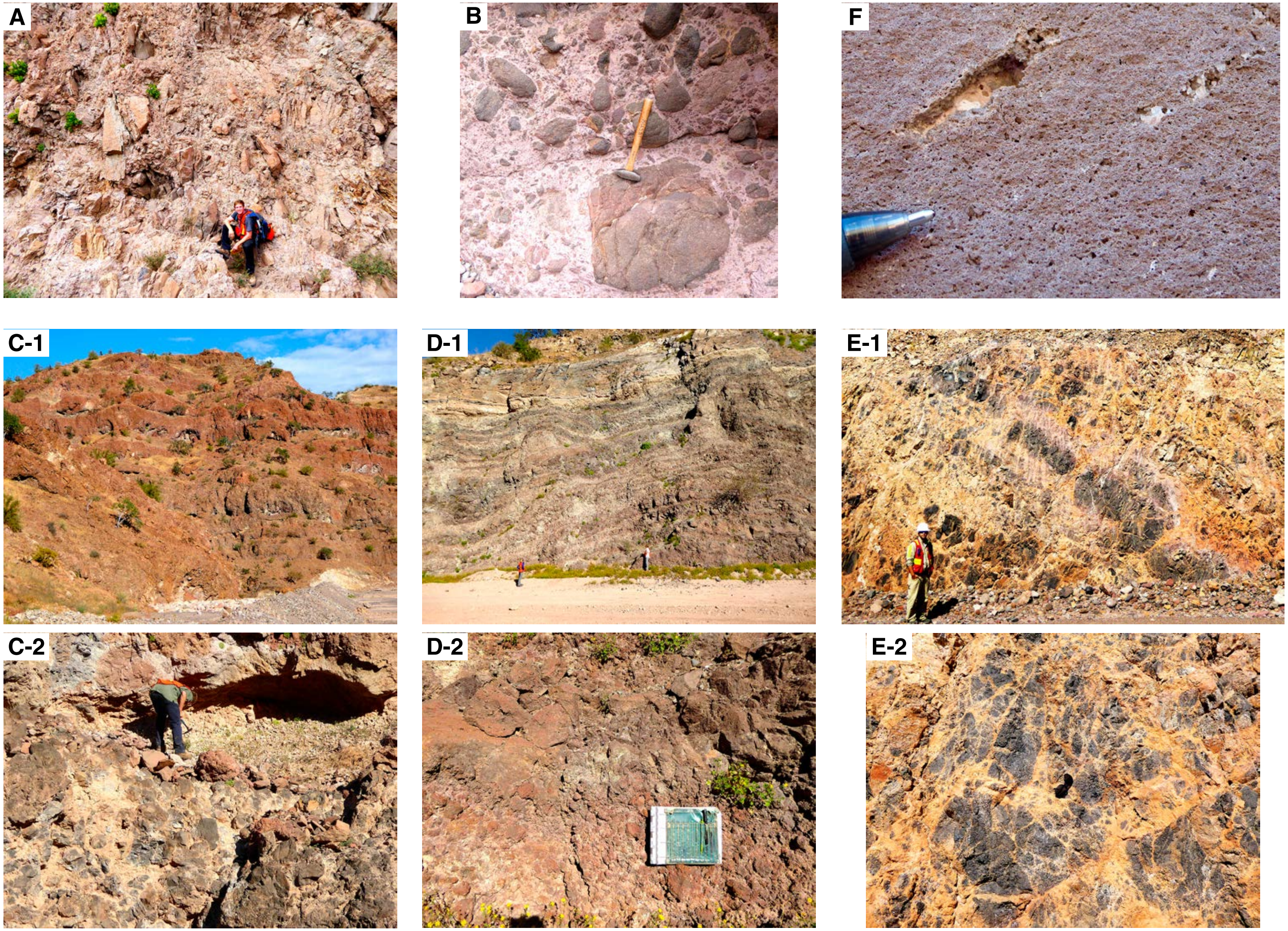

Figure 6. Representative outcrop photos of volcanic lithofacies. See Item S6 (text footnote 1) for a more complete catalog of outcrop photos, with more detailed information (e.g., map unit name, chemistry, age, and detailed outcrop description). (A) Trachyandesite lava dome mantled by breccia with blocks up to 1 m. (B) Andesite block-and-ash-flow tuff. (C-1) Thick andesite lavas (~10 m each), with alternating resistant coherent interiors and recessive flow breccias. (C-2) Close-up of flow-top breccia on thick andesite lavas, with blocks up to 0.5 m, and sandstone infiltrations and beds. (D-1) Thin scoriaceous basaltic trachyandesite lavas (<2–3 m thick). (D-2) Close-up of flow-top scoria lapilli and small blocks on a thin basaltic trachyandesite lava. (E-1) Andesite peperite intrusion, forming variably disrupted sills within a sedimentary rock host. (E-2) Close-up of peperite intrusion, showing andesite blocks with jigsaw clast texture dispersed in tan volcaniclastic sandstone (sunglasses for scale). (F) Trachyandesite hypabyssal intrusion, showing miarolitic cavities of irregular shape with crystals projecting into the cavities, partially filling them.

Santa Rosalía south geologic map (Fig. 3) was mapped on Google Earth base map with Digital Globe imagery from 2016. Maps from Google Earth use the WGS 1984 coordinate system. Additionally, 30 m contour lines derived from ASTER GDEM V2.0 courtesy of Ministry of Economy, Trade, and Industry (METI) and National Aeronautics and Space Administration (NASA). Field mapping and data were entered at a variety of spatial scales using a tablet with GPS and the FieldMove program. Strikes and dips were taken with both Brunton compass and FieldMove Clino at all locations. Google Earth KMZ files are provided in Item S9 (footnote 1), with map layers and map units, sample locations, strike and dip measurements, and faults.

ORGANIZATION

Volcanic lithofacies (e.g., lavas, block-and-ash-flow tuffs, ignimbrites, etc.) are described in the first section of this paper. Volcanic-volcaniclastic terminology follows that of Fisher and Schmincke (1984). Lithofacies repeat, but they are separated into distinct map units (Table 1) using contact relations and variations in chemistry, mineralogy, textures, and $^{40}Ar-^{39}Ar$ geochronologic ages. These map units are described in the second section and grouped by chemistry into three basic categories (calcalkaline, rift transitional, and high-magnesian andesites), but discussion of the geochemistry is deferred until after the map units are described.

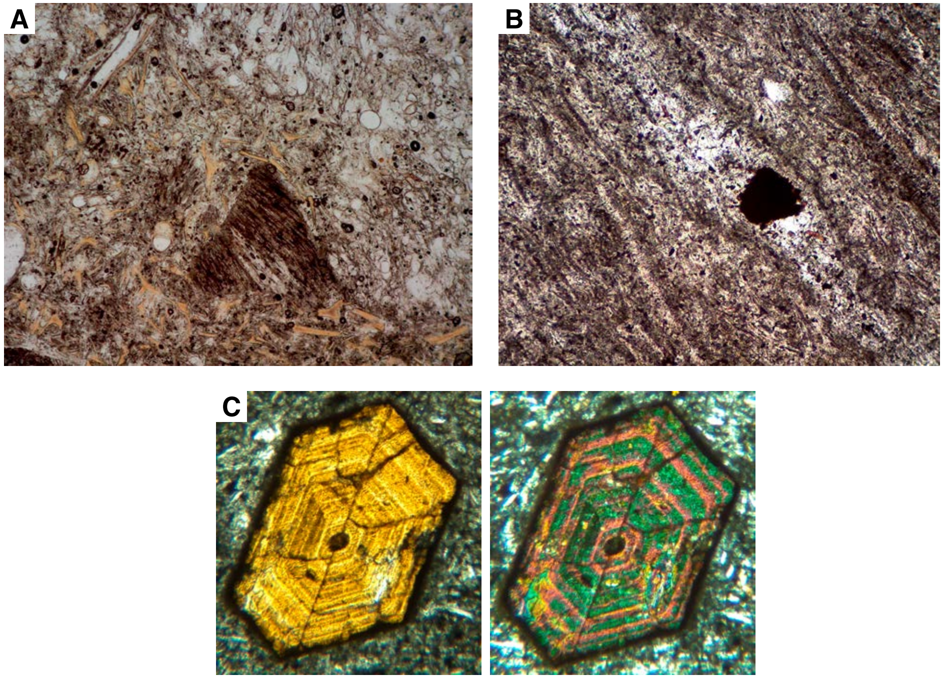

Figure 7. Selected photomicrographs; see Supplemental Item S7 (text footnote 1) for a more complete catalog of photomicrographs, including all samples dated by $^{40}Ar-^{39}Ar$. (A) Pink nonwelded trachydacite ignimbrite (tuff of El Morro), composed of pumice lapilli and bubble-wall shards. Center of photo is an angular welded ignimbrite lithic clast (plain polarized light, field of view 6 mm). (B) Purple welded rhyolite ignimbrite (tuff of El Morro), with compacted pumice, and sintered and flattened bubble-wall shards. Opaque mineral may be hematite replacement of part of a pumice (plain polarized light, field of view 6 mm). (C) Plain polarized (1) and cross polarized light (2), respectively: high-magnesian trachyandesite hypabyssal intrusion. Finely zoned hornblende phenocryst with thin opaque rim. Field of view 2 mm.

VOLCANIC LITHOFACIES

We mapped the following volcanic lithofacies in the Santa Rosalía area: lava domes, block-and-ash-flow tuffs, lavas, peperites, hypabyssal intrusions, and ignimbrites. Lava domes are recognized as coherent, compositionally homogeneous bodies with high aspect ratio (i.e., thick and highly lenticular), mantled by coarse breccias of the same composition (Fig. 6A). These domes can commonly be mapped down-section into intrusions that crosscut stratigraphy. Block-and-ash-flow tuffs consist of unsorted, nonstratified deposits of block- to lapilli- to ash-sized clasts, all of the same composition (Fig. 6B). These deposits are widely regarded to result from non-explosive collapse of lava domes or lava flow fronts (e.g., Fisher et al., 1980; Sparks, 1997; Freundt et al., 2000). Lavas are distinguished from intrusions by the presence of flow-top breccias or vesiculated tops that form layers. Lavas may be further subdivided by textural characteristics; in this area, we subdivide them by marked differences in thickness. Thick lavas form stratified sections with individual flows ~10 m thick, with coherent intervals separated by flow breccias with large blocks (Fig. 6C). Thin lavas form stratified sections with individual flows less than 2–3 m thick, with coherent intervals separated by scoria lapilli and small blocks (Fig. 6D). Peperite intrusions consist of glassy (quenched) blocks with jigsaw clast texture dispersed in a sedimentary host (Fig. 6E). Hypabyssal intrusions form coherent, homogeneous bodies that crosscut stratigraphy; the example shown in Figure 6F has miarolitic cavities. Ignimbrites consist of pumice (light-colored) or scoria (dark-colored) blocks in a matrix of bubble-wall shards of the same composition. They form thick massive, unsorted deposits and commonly contain volcanic rock fragments and broken crystals. Ignimbrites are commonly laterally extensive, so they are used as regional-scale stratigraphic

TABLE 1A. SANTA ROSALÍA NORTH (FIGS. 2 AND 3)—UNITS GROUPED GEOGRAPHICALLY

Geochemical designation (plus age)	Map sample no.	Map unit name	Outcrop description	Petrography	Sample name
Cerro Sombrero Montado (Fig. 3)					
Rift transitional 8.84 ± 0.16 (whole rock)	SR 14-5	Andesite lava	>80-m-thick (top eroded) flow-banded lava, vesicular, largely coherent with minor flow breccia.	<5% plagioclase phenocrysts, some skeletal and sieve textured, <2 mm long. 1% ferruginous-altered hornblende. Plagioclase microlite groundmass with interstitial very small clinopyroxene.	Phenocryst-poor andesite lava
No chemistry (too many lithics)	SR 14-4	Lithic pumice lapilli tuff	Hornblende pumice lapilli tuff with volcanic rock fragments. Overlain by the andesite lava (SR 14-5).	60% pristine pumice shreds, 15% pristine broken hornblende up to 5 mm, 5% plagioclase up to 3 mm, and 20% volcanic rock fragments.	Hornblende lithic pumice lapilli tuff
Cerro Juanita (Fig. 3)					
Rift transitional 9.66 ± 0.21 (whole rock)	SR 14-1	Basaltic andesite lava	>100-m-thick lava with basal breccia (top eroded), locally flow-banded.	Phenocryst-poor (3%), with 1% plagioclase, 1% ferruginous-altered hornblende, and 1% clinopyroxene. Fresh groundmass with flow-aligned plagioclase microlites.	Phenocryst-poor basaltic andesite lava
Rift transitional	SR 14-2	Basaltic andesite lava	Same >100-m-thick lava as above (sample SR 14-1), downsection from it.	20% fresh plagioclase, up to 3 mm, 5% clinopyroxene some in glomerocrysts with plagioclase, 2% ferruginous-altered hornblende. Groundmass with flow-aligned plagioclase microlites.	Hornblende clinopyroxene basaltic andesite lava
Rift transitional	SR 14-3	Basalt lava	30-m-thick lava, resting on stratified lapilli tuff and overlain by basaltic andesite lava (SR 14-2 and 14-1).	60% plagioclase laths ranging from microlites to 2 mm long, oriented randomly with interstitial microcrystalline clinopyroxene, plus 5% red hematite <1 mm, and opaques.	Plagioclase-rich basalt lava
Arroyo Purgatorio (Fig. 3)					
Rift transitional	SR 17-2	Basaltic andesite lava	Lava with flow breccia.	60% randomly oriented plagioclase laths ranging from microlites to phenocrysts <0.5 mm (2%). 2% altered mafic phenocrysts <4 mm.	Basaltic andesite lava
Calcalkaline	SR 17-1	Dacite lava or intrusion	Lava or intrusion. Too small to map separately.	Phenocryst-poor (3%); unaltered clinopyroxene phenocrysts (<2 mm) and glomerocrysts in a groundmass of small flow-aligned plagioclase microlites. Trace altered hornblende.	Clinopyroxene dacite lava or intrusion
El Morro (Fig. 3)					
Rift transitional	Clast	Pink nonwelded lithic rhyolite to trachydacite ignimbrite	Angular block of purple welded ignimbrite in the pink nonwelded lithic rhyolite to trachydacite ignimbrite.	Sintered glass shards partially pseudomorphed by hematite. Compacted pumice replaced by spherulites and fibrous quartz. No rock fragments and rare plagioclase phenocrysts.	Clast of silicified purple welded rhyolite ignimbrite within pink nonwelded ignimbrite
Rift transitional	SR 15-4	Purple welded rhyolite ignimbrite	Lithic-free, densely welded, aphyric, purple ignimbrite. Locally rests on pink nonwelded lithic ignimbrite.	Aphyric, with compacted pumice and sintered bubble-wall shards. No lithics.	Aphyric lithic-free rhyolite welded ignimbrite
Rift transitional	SR 15-5	Pink nonwelded lithic rhyolite to trachydacite ignimbrite	Pumice-rich layer at top of the pink nonwelded lithic ignimbrite.	Aphyric, nonwelded pumice lapillistone (uncompacted) with <5% volcanic rock fragments.	Trachydacite pumice lapillistone
Rift transitional	SR 15-6	Pink nonwelded lithic rhyolite to trachydacite ignimbrite	One single pumice from a pumice lens on top of the upper lava within the pink nonwelded lithic ignimbrite.	Nearly aphyric: <1% small (<0.5 mm) plagioclase.	Trachydacite pumice
Rift transitional lava 9.69 ± 0.12 (groundmass)	SR 15-8	Basaltic trachyandesite lavas interstratified with pink nonwelded lithic ignimbrite	Upper of two lavas within the pink nonwelded lithic ignimbrite. Coherent interior, surrounded by thick breccias, with underlying and overlying reworked tuff and/or tuffaceous sandstone lenses.	25% plagioclase, some sieve-textured to skeletal, up to 6 mm long. 2% small (mostly <0.5 mm) clinopyroxene. Felted plagioclase microlite groundmass.	Basaltic trachyandesite lava

(*continued*)

TABLE 1A. SANTA ROSALÍA NORTH (FIGS. 2 AND 3)—UNITS GROUPED GEOGRAPHICALLY (*continued*)

Geochemical designation (plus age)	Map sample no.	Map unit name	Outcrop description	Petrography	Sample name
El Morro (Fig 3) (*continued*)					
Rift transitional	El Morro	Pink nonwelded lithic rhyolite to trachydacite ignimbrite	Pink nonwelded Ignimbrite with abundant lithics.	Excellent vitroclastic texture: aphyric pumices well preserved between rock fragments. Matrix has 5% plagioclase crystals up to 2 mm. Lithics are silicic to intermediate volcanic rock fragments, including welded ignimbrite clasts.	Nonwelded rhyolite lithic ignimbrite
Rift transitional	Montado-02 CORE SAMPLE	Pink nonwelded lithic rhyolite to trachydacite ignimbrite	Ignimbrite with sparse (5%) accidental volcanic rock fragments. Collared at 88', sampled at depth of 79' (9' above sea level).	Less than 1% small (<0.5 mm) plagioclase. Abundant (~30%) relict glass fragments, some with perlitic fracture. Faint eutaxitic texture (flattened pumice).	Nearly aphyric rhyolite ignimbrite
Rift transitional	Montado-07 CORE SAMPLE	Pink nonwelded lithic rhyolite to trachydacite ignimbrite	Pink nonwelded Ignimbrite with no rock fragments. Collared at 97', sampled at depth of 180' (83' below sea level).	5% plagioclase phenocrysts (up to 2 mm) and glomerocrysts (up to 6 mm). No glass preserved. No rock fragments.	Crystal-poor rhyolite ignimbrite
East of Curuglu fault (Fig. 3)					
Calcalkaline 10.83 ± 0.95 (groundmass)	SR 08-4	Andesite lava	Lava with abundant flow breccia, resting on tuff of Curuglu.	25% plagioclase up to 2 mm, 5% clinopyroxene up to 3 mm, 2% relict hornblende, in a very fine-grained groundmass.	Hornblende clinopyroxene andesite lava
Calcalkaline	SR 08-1	Basaltic andesite to andesite tuff of Curuglu	Black clasts in tuff of Curuglu.	Aphyric.	Aphyric andesite clast
Calcalkaline	SR 08-2	Basaltic andesite to andesite tuff of Curuglu	Scoria lapilli tuff matrix with minimal volcanic clasts.	25% plagioclase, 15% clinopyroxene up to 3 mm in glomerocrysts. Scoria lapilli consist of orange relict glass with plagioclase microlites, abundant vesicles and bubble-wall shards.	Clinopyroxene basaltic andesite ignimbrite
Calcalkaline	SR 08-3	Basaltic andesite to andesite tuff of Curuglu	Scoria block from tuff of Curuglu.	Aphyric.	Andesite scoria block
Mina Victoria (Fig. 3)					
Calcalkaline	SR 12-6	Thin scoriaceous basaltic trachyandesite lavas	Thin (1–2 m) coherent vesicular lavas alternating with thick (1–3 m) scoriaceous flow breccias.	3% ferruginous-altered hornblende in a groundmass of flow-aligned plagioclase microlites with interstitial altered hornblende.	Hornblende basaltic trachyandesite lava
Calcalkaline	SR 12-5	Thick andesite lavas	Sample from a coherent flow interior at top of section.	5% euhedral ferruginous-altered hornblende (2 mm) and 2% clinopyroxene (up to 2 mm) in a microlitic groundmass. Unusual for its lack of plagioclase phenocrysts.	Clinopyroxene hornblende andesite lava
Calcalkaline 10.1 ± 0.9 (groundmass)	SR 12-2	Thick andesite lavas	Sample from coherent interior of a lava in the middle of the thick andesite lavas section.	10% plagioclase phenocrysts and glomerocrysts up to 2 mm, 10% clinopyroxene glomerocrysts and phenocrysts up to 4 mm, 5% ferruginous-altered hornblende. Groundmass of flow-aligned plagioclase microlites.	Hornblende clinopyroxene andesite lava
Calcalkaline	SR 09-7	Thick andesite lavas	Sample is a block from flow breccia in the lower part of thick andesite lavas section. This section rests on the trachyandesite lava dome.	Abundant (~30%) small (0.5 mm) plagioclase phenocrysts, large (3 mm) clinopyroxene 10% some with skeletal texture.	Clinopyroxene andesite lava
Calcalkaline	SR 09-5	Trachyandesite lava dome	Block from breccia mantling the top of the trachyandesite lava dome, overlain by the thick andesite lavas map unit.	10% clinopyroxene (2–3 mm), 5% plagioclase (up to 5 mm), and 5% relict hornblende phenocrysts, in a groundmass of flow-aligned plagioclase microlites with interstitial altered hornblende.	Hornblende clinopyroxene trachyandesite lava dome breccia

(*continued*)

TABLE 1A. SANTA ROSALÍA NORTH (FIGS. 2 AND 3)—UNITS GROUPED GEOGRAPHICALLY (*continued*)

Geochemical designation (plus age)	Map sample no.	Map unit name	Outcrop description	Petrography	Sample name
Mina Victoria (Fig. 3) (*continued*)					
Calcalkaline 13.81 ± 0.10 (groundmass)	SR 12-4	Trachyandesite lava dome	Gray-green flow-banded lava dome interior.	10% clinopyroxene in glomerocrysts ≤5 mm, 5% plagioclase phenocrysts (<2 mm) and 5% relict red hornblende phenocrysts (<1 mm), in a groundmass of flow-aligned plagioclase microlites with interstitial altered hornblende.	Hornblende clinopyroxene trachyandesite lava dome interior
Calcalkaline	SR 09-4	Andesite peperite intrusion	Gray-green intensely flow-jointed hypabyssal intrusion.	5% plagioclase glomerocrysts (up to 3 mm) 7% large clinopyroxene (4 mm), 5% small ferruginous-altered hornblende (1 m).	Hornblende clinopyroxene basaltic andesite hypabyssal intrusion
Calcalkaline	PEP	Andesite peperite intrusion	Black glassy blocks with jigsaw clast texture dispersed in volcaniclastic sandstone.	3% clinopyroxene phenocrysts ≤1 mm and glomerocrysts up to 4 mm, 1% red hornblende (oxyhornblende?) (0.5 mm). Groundmass of scattered plagioclase microlites set in black glass (partially devitrified). 20% vesicles with irregular shapes.	Hornblende clinopyroxene andesite peperite intrusion
Mina Santa Teresa (Fig. 3)					
Calcalkaline 13.21 ± 0.21 (groundmass)*	SR 09-1	Trachyandesite lava dome, and andesite block-and-ash-flow tuffs and lavas	Hornblende clinopyroxene andesite lava upsection from the block-and-ash-flow tuff (SR 08-5).	5% clinopyroxene to 4 mm, 5% relict hornblende pseudomorphed by opaque mineral (up to 4 mm), 5% plagioclase in glomerocrysts to 6 mm (some with clinopyroxene).	Hornblende clinopyroxene andesite lava
Calcalkaline	SR 08-5	Trachyandesite lava dome, and andesite block-and-ash-flow tuffs and lavas	Block from a block-and-ash-flow tuff upsection from the coherent lava dome with dome breccia (SR 08-6).	15% plagioclase to 6 mm, 5% ferruginous-altered hornblende, 5% clinopyroxene. Groundmass finer grained and more hematized than 08-6.	Hornblende clinopyroxene andesite block-and-ash-flow tuff
Calcalkaline 13.08 ± 0.11 (groundmass)	SR 08-6	Trachyandesite lava dome, and andesite block-and-ash-flow tuffs and lavas	Coherent interior of lava dome, mantled by breccias.	10% plagioclase phenocrysts (<2 mm) and glomerocrysts (<4 mm), 5% clinopyroxene phenocrysts (1–2 mm) and 5% relict hornblende phenocrysts (1 mm). Groundmass of large flow-aligned plagioclase microlites with small interstitial clinopyroxene.	Hornblende clinopyroxene trachyandesite lava dome interior
West of Curuglu fault (Fig. 3), stratigraphic position and age unknown					
Calcalkaline	SR 09-2	Hematized basaltic andesite lavas	Flow-banded with flow breccia, hematized.	5% fresh plagioclase <2 mm, 3% ferruginous- and opaque-altered hornblende up to 3 mm, 2% clinopyroxene <2 mm. Groundmass hematized.	Clinopyroxene hornblende basaltic andesite lava
Northern Core Localities (Fig. 2), stratigraphic position and age unknown					
Calcalkaline	LS-10	Not mapped	Collared at 320', sampled at depth of 57' (262' above sea level).	20% plagioclase phenocrysts up to 1 mm, 3% hornblende phenocrysts up to 2 mm, opaque rims. 1% clinopyroxene phenocrysts up to 1 mm. Groundmass of randomly oriented plagioclase laths in devitrified glass.	Clinopyroxene hornblende plagioclase porphyry dacite lava or intrusion
Calcalkaline	LS-08	Not mapped	Collared at 325', sampled at depth of 63' (263' above sea level).	Same as LS-08	Clinopyroxene hornblende plagioclase porphyry dacite lava or intrusion
Mina Caopas Gypsum Mine (Fig. 2), stratigraphic position and age unknown					
Calcalkaline	SR 10-1	Not mapped	Sample from coherent interior of a lava mantled by breccia and overlain by gypsum (base not exposed).	Crystal-rich (40%) with 30% plagioclase up to 2 mm, 10% clinopyroxene up to 3 mm, and 5% smaller ferruginous-altered hornblende (5%).	Hornblende clinopyroxene plagioclase porphyry basaltic andesite lava

*Note: Overlaps within error with sample SR 08-6.

TABLE 1B. SANTA ROSALÍA SOUTH (FIG. 4)

Geochemical designation (plus age)	Map sample no.	Map unit name	Outcrop description	Petrography	Sample name
High-magnesian trachyandesite lavas and intrusions					
High-magnesian andesite 6.06 ± 0.27 (hornblende)	SL 08-1	High-magnesian trachyandesite intrusion	Intrusion crosscutting calcalkaline volcanic rocks. Hornblende in dark-gray groundmass, miarolitic cavities.	10% hornblende phenocrysts up to 2 mm long, largely unaltered, but some with thin opaque rims, 3% clinopyroxene phenocrysts (<1 mm) and glomerocrysts in a groundmass of plagioclase microlites with weak flow alignment. No plagioclase phenocrysts.	Clinopyroxene hornblende high-magnesian trachyandesite hypabyssal intrusion
High-magnesian andesite	SL 08-3	High-magnesian trachyandesite intrusion	Topographically lower (deeper) in same intrusion as sample SL 08-1. Hornblende in dark-gray groundmass, miarolitic cavities.	10% hornblende phenocrysts up to 2 mm long, flow-aligned, with thicker opaque rims than sample SL08-1. 3% clinopyroxene phenocrysts and glomerocrysts. Fine-grained microlitic groundmass. No plagioclase phenocrysts.	Clinopyroxene hornblende high-magnesian trachyandesite hypabyssal intrusion with miarolitic cavities
High-magnesian andesites	SL 10-1	High-magnesian trachyandesite intrusion	Separate intrusion from samples SL 08-1 and 08-3. Crosscuts calcalkaline lavas. Hornblende in dark-gray groundmass.	15% hornblende phenocrysts and needles largely replaced by opaques, largely flow-aligned in microlitic plagioclase flow-aligned groundmass. No clinopyroxene or plagioclase phenocrysts.	Hornblende high-magnesian trachyandesite hypabyssal intrusion
High-magnesian andesite	SL 08-7	High-magnesian trachyandesite lava	Lava with thick flow-top breccia. Upsection from calcalkaline lavas.	20% plagioclase phenocrysts (≤2 mm). 10% clinopyroxene phenocrysts (≤3 mm) and glomerocrysts (≤5 mm). Plagioclase-clinopyroxene glomerocrysts ≤6 mm. 5% altered hornblende. Coarse-grained microlitic groundmass with flow alignment.	Hornblende clinopyroxene high-magnesian trachyandesite lava
High-magnesian andesite	SL 08-5	High-magnesian trachyandesite lava	Flow-banded lava. Upsection from calcalkaline lavas.	10% flow-aligned relict hornblende up to 6 mm long almost entirely replaced by opaques. ~3% small altered clinopyroxene. No plagioclase phenocrysts. Amygdules. Hematized.	Clinopyroxene hornblende high-magnesian trachyandesite lava
Calcalkaline volcanic rocks					
Calcalkaline	SL 10-3	Andesite block-and-ash-flow tuffs	Flow-banded blocks up to 2 m in a matrix of lapilli and ash of the same composition. Includes minor thin (<1 m) intrusions with fluidal margins.	Abundant (30%) plagioclase phenocrysts up to 3 mm (and minor glomerocrysts), plus 10% clinopyroxene crystals up to 2 mm and glomerocrysts up to 4 mm, in a cryptocrystalline groundmass. No flow alignment.	Crystal-rich clinopyroxene andesite block-and-ash-flow tuff
Calcalkaline	SL 16-4	Andesite block-and-ash-flow tuffs	Block from an andesite block-and-ash-flow tuff.	Identical to sample SL 10-3 in thin section.	Crystal-rich clinopyroxene andesite block-and-ash-flow tuff
Calcalkaline 10.11 ± 0.14 (groundmass)	SL 08-4	Andesite lavas	Flow-banded lava with flow breccias.	Abundant (25%) plagioclase phenocrysts up to 2 mm and minor glomerocrysts up to 3 mm, 15% clinopyroxene crystals up to 2 mm and glomerocrysts up to 5 mm, in a cryptocrystalline groundmass. No flow alignment.	Crystal-rich clinopyroxene andesite lava
Calcalkaline	SL 12-2	Andesite lavas	Coherent lava passing gradationally upward into flow breccia. Sample from coherent part.	20% plagioclase phenocrysts up to 2 mm and glomerocrysts up to 5 mm, 10% clinopyroxene phenocrysts up to 3 mm. Plagioclase microlites and opaques in cryptocrystalline groundmass.	Clinopyroxene andesite lava
Calcalkaline	SL 12-3	Dacite block-and-ash-flow tuff (within the andesite lavas)	Light-gray recessive-weathering block-and-ash-flow tuff, 15 m thick, underlain and overlain by resistant clinopyroxene andesite lavas. Sample is from a block.	Abundant (35%) plagioclase phenocrysts, very fresh, many very finely zoned, rare sieve textures; 2% hornblende phenocrysts (1 mm) mainly replaced by opaques.	Plagioclase porphyry hornblende dacite block-and-ash-flow tuff
Calcalkaline	SL 13-1	Andesite lavas	Flow-banded lava with flow breccia.	25% plagioclase up to 3 mm, glomerocrysts up to 5 mm; clinopyroxene up to 2 mm, also in glomerocrysts with plagioclase up to 10 mm. Groundmass has very small plagioclase microlites in darker (former glass?) and lighter (devitrified?) flow bands. Flow alignment of phenocrysts and microlites.	Clinopyroxene andesite lava
Calcalkaline	SL 13-4	Red hornblende andesite lava (within the andesite lavas)	Lava with flow breccia, red-colored.	10% hornblende phenocrysts up to 3 mm with zoning and opaque (hematite?) rims and zones; 5% plagioclase phenocrysts up to 2 mm. Flow-aligned plagioclase microlites in cryptocrystalline groundmass.	Hematized hornblende andesite lava
Calcalkaline	SL 15-2	Andesite lavas	Lava with flow breccia.	Phenocryst-poor: 3% clinopyroxene up to 2 mm, in groundmass of flow-aligned plagioclase microlites.	Crystal-poor clinopyroxene andesite lava

markers (e.g., Busby et al., 2005; Murray et al., 2013; Busby et al., 2018a). For this reason, we describe this lithofacies in detail below, in stratigraphic and geochronological context.

STRATIGRAPHY, ^{40}Ar-^{39}Ar GEOCHRONOLOGY, AND U-Pb ZIRCON GEOCHRONOLOGY

The Santa Rosalía north area is subdivided into outcrop areas (e.g., Cerro Sombrero Montado, Cerro Juanita, El Morro, etc., Fig. 3, Table 1A) separated by sedimentary rocks of the Santa Rosalía basin (Fig. 2). The Santa Rosalía south area forms one contiguous outcrop area (Fig. 4). Within outcrop areas, map units are shown in stratigraphic order on the map keys (Figs. 3 and 4); however, none of the map units are continuous from one outcrop area to the next. Therefore, the composite stratigraphy shown on Figure 3 and Table 1A was constructed using the ^{40}Ar-^{39}Ar ages shown on the map key and Figure 5.

Table 1 provides an outline for the description of map units, grouping the map units by outcrop area and summarizing outcrop and petrographic characteristics of 47 samples. The units described in Table 1A (Santa Rosalía north, Fig. 3) are described first because that area ranges to older ages than rocks of Santa Rosalía south (Table 1B), which ranges to younger ages (Fig. 4). Compositional names (e.g., andesite and basaltic trachyandesite) were assigned using major- and trace-element data (Item S2 [footnote 1]), and we group these by geochemical characteristics into the following geochemical designations: (1) calcalkaline, (2) rift transitional rocks, further divided into ignimbrites and lavas, and (3) high-magnesian andesites. The distribution of rocks with these geochemical designations is shown in the insets of the geologic maps (Figs. 3 and 4).

^{40}Ar-^{39} Ar ages are summarized in stratigraphic order, grouped and color-coded by geochemical designation, in Figure 5. Age spectra and $^{36}Ar/^{40}Ar$ versus $^{39}Ar/^{40}Ar$ correlation diagrams are shown in Figures 8A and 8B, respectively. Item S3 contains a summary table of the ^{40}Ar-^{39}Ar results, and for each sample, it presents a table with relevant ^{40}Ar-^{39}Ar, age spectra, $^{37}Ar_{Ca}/^{39}Ar_K$ diagram, and $^{36}Ar/^{40}Ar$ versus $^{39}Ar/^{40}Ar$ correlation diagram.

Selected outcrop photos (Fig. 6) are presented herein. A more complete set is presented in Item S6, in order to help the reader visualize field characteristics. A complete set of photomicrographs is presented in Item S7 to provide data on volcanic textures, minerals, and alteration. Photomicrographs are provided for all dated samples (Item S7). Unless otherwise noted, all samples have plagioclase; the other mineral names are given in order of increasing abundance on Table 1 (least abundant mineral first, as is standard). In this section, the map unit names shown on Figures 3 and 4 and Table 1 are written in italics, for ease of reference.

Santa Rosalía North

Rocks of Uncertain Stratigraphic Position

Three geographic areas are arbitrarily placed at the base of Table 1A because their age is unknown.

The Mina Caopas gypsum lies in the north end of the Santa Rosalía sedimentary basin (Fig. 2) and is ~100 m thick, making it one of the biggest gypsum producers in the world. At one locality in the bottom of an arroyo, the gypsum rests on a lobate body of *basaltic andesite lava* (Table 1). This body has abundant plagioclase, so we name it a hornblende clinopyroxene plagioclase porphyry to emphasize that fact (sample SR 10-1, Table 1). It has a coherent interior mantled by flow breccia and passes laterally into a block-and-ash-flow tuff with the same mineralogy and blocks up to 1.5 m in size (Items S6A-1 and S6A-2 [footnote 1]). This lava is calcalkaline (Table 1). Therefore, it is not likely that it would yield a useful maximum age on the base of the gypsum, since it is likely to be >12 Ma in age, although calcalkaline volcanism has recurred since subduction ended, as discussed above.

The northern core localities (cores LS-08 and LS-10, Fig. 2) were drilled beneath the Santa Rosalía basin sedimentary fill. They consist of *coherent dacite* (calcalkaline); LS-10 and LS-08, Table 1A), and may either represent lava with the flow-top breccia eroded away or hypabyssal intrusions. These samples are the only dacite lavas or intrusions we have found in the Santa Rosalía area, except for a small body of coherent calcalkaline clinopyroxene dacite at Arroyo Purgatorio (sample SR 17-1, Fig. 3; Table 1A).

The *hematized basaltic andesite lavas* map unit forms an extensive outcrop west of the Curuglu fault (Fig. 3). It is an ~200-m-thick section of calcalkaline lavas (sample SR 09-2, Table 1A). They are bright red (Item S6B) and are undated because of the alteration. The section has the same strike and dip as the top of the Mina Santa Teresa section (described below), which may underlie it; but because it is so much more altered (and undated), we did not include it in the Mina Santa Teresa section.

Mina Santa Teresa

The Mina Santa Teresa section is mapped as one unit: *trachyandesite lava dome and andesite block-and-ash-flow tuffs and lavas* (calcalkaline in composition) with internal stratigraphic variation described here (Fig. 3 and Table 1A).

The base of the Mina Santa Teresa section is a hornblende clinopyroxene trachyandesite lava dome with a coherent interior (sample SR 08-6, Table 1A, Item 7A), mantled by breccias (Fig. 6A). The best age estimate of sample SR 08-6 is the plateau age of 13.08 ± 0.11 Ma calculated with the weighted mean of eight consecutive fractions of the step-heating experiment performed with a groundmass sample (Fig. 8A-3). The data used to calculate the plateau age cluster close to the x-intercept on the ($^{36}Ar/^{40}Ar$) versus ($^{39}Ar/^{40}Ar$) correlation diagram; to calculate the straight line fraction, "g" was ignored, yielding an isochron age of 13.03 ± 0.36 Ma (Fig. 8B-3). This less precise isochron age is in agreement within 1σ errors with the plateau age.

The lava dome passes gradationally upward (northward) into hornblende clinopyroxene andesite block-and-ash-flow tuff (sample SR 08-5, Table 1A). This is a nonstratified deposit of dense (nonvesicular) angular blocks up to 1 m across,

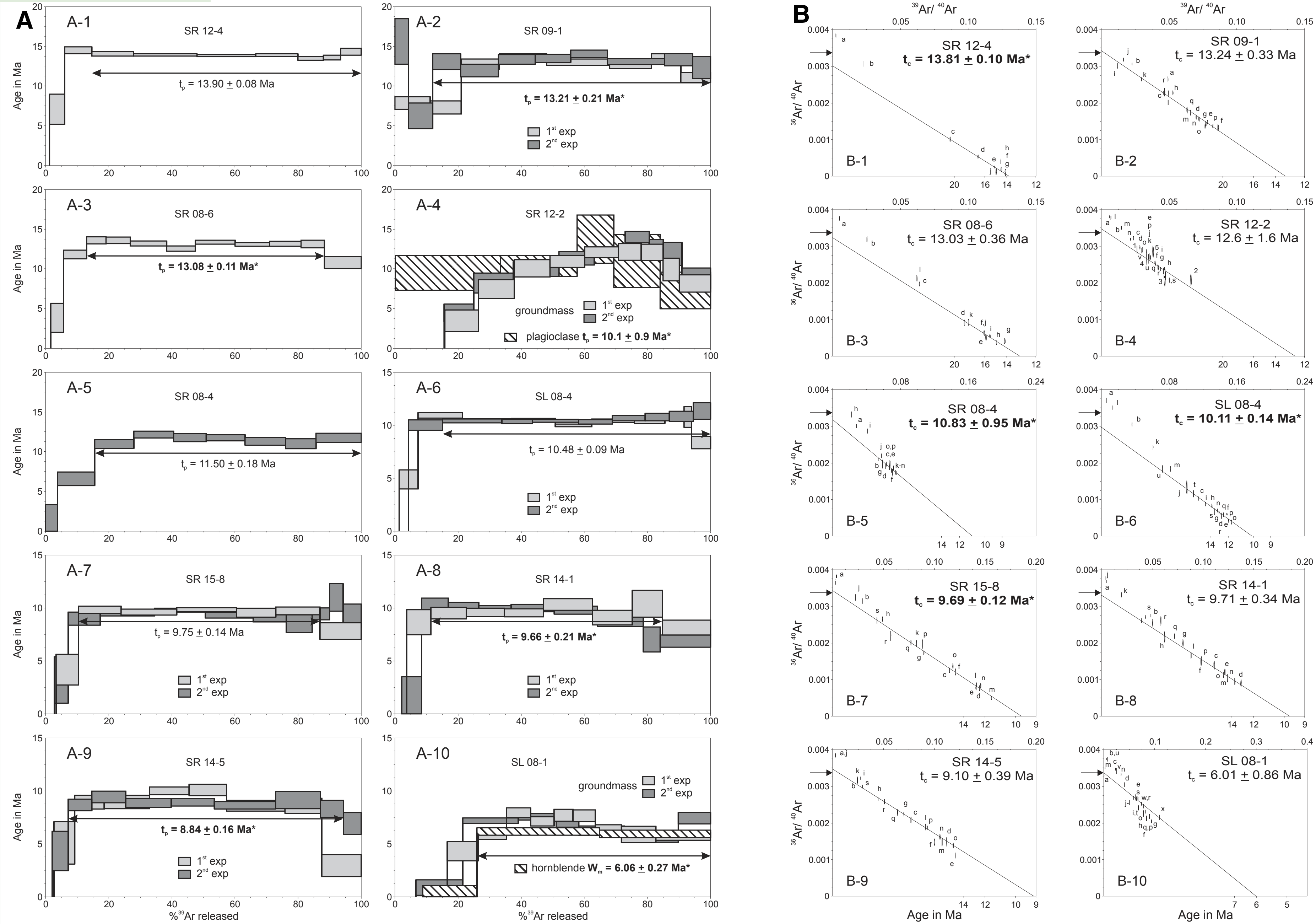

Figure 8. ^{40}Ar-^{39} Ar plots: (A) plateau ages and (B) isochron ages. Samples are plotted on Figures 3 and 4 and summarized on Figure 5. Methods are given in Item S1 and data are given in Item S3 (text footnote 1).

supported in a matrix of lapilli tuff and tuff of the same composition (Fig. 6B). The block-and-ash-flow tuff is overlain by a hornblende clinopyroxene andesite lava (sample SR 09-1, Table 1A), which forms the top of the section. Plagioclase and clinopyroxene are fresh, and hornblende is altered (Item 7-B [footnote 1]). This hornblende clinopyroxene andesite lava is dated at 13.21 ± 0.21 Ma (sample SR 09-1, Fig. 5). Two ^{40}Ar-^{39}Ar experiments were performed on the same groundmass concentrate of this sample. The experiments yielded reproducible results with a well-defined plateau age of 13.21 ± 0.21 Ma (Fig. 8A-2) for 88% of the ^{39}Ar released in eight fractions. The plateau age is statistically equal to the isochron age (Fig. 8B-2), calculated from data for the combined fractions of the two experiments performed.

The ages of sample SR 08-6, at the base of the Mina Santa Teresa section, and sample SR 09-1, at its top, overlap within two sigma errors (Fig. 5).

Mina Victoria

We mapped four units in the Mina Victoria area (Fig. 3), all calcalkaline (Table 1A). These are described in stratigraphic order.

Andesite peperite intrusion forms the base of the Mina Victoria (sample PEP, Table 1). It has black, glassy andesite blocks showing jigsaw clast texture partially dispersed in tan volcaniclastic sandstone, indicating interaction of the magma with wet sediment (Fig. 4E; Items S6D-1–S6D-3 and Item S7C). Sandstone injections into cracks of widely varying orientations in the blocks indicate that steam explosions were generated as the magma mixed with wet sediment, in places as sills. This intrusion appears to pass gradationally upward into the overlying *trachyandesite lava dome* map unit, which has the same mineralogy but slightly different chemistry (Table 1A; Item S2).

Trachyandesite lava dome is mapped as one unit (Fig. 3), but the coherent lava dome interior (sample SR 12-4) and the lava dome breccia (sample SR 09-5) are described separately in Table 1A. The coherent interior and the breccia have the same composition, mineralogy, and flow-banded texture (Items S6D-4 and S6D-5 [footnote 1]). The dome interior is devitrified to a gray-green color, with intense flow foliation at its base, becoming less jointed upward but retaining strong flow banding. The coherent dome interior rocks pass gradationally upward into the lava dome breccias, with breccias locally intruded by coherent material. The dome interior was sampled for geochronology; a photomicrograph of the sample is provided in Item 7D. Breccias of the lava dome are conformably overlain by the *thick andesite lavas* map unit.

The *thick andesite lavas* map unit (Fig. 3 and Table 1A) consists of ~10-m-thick lavas, with coherent lava interiors alternating with coarse, nonvesicular flow breccias (Items SD6 and SD6-7 [footnote 1]). All of the lavas in this map unit are andesite but vary in their proportions of clinopyroxene, hornblende, and plagioclase (samples SR 09-7, SR12-2, and SR 12-5, Table 1A). Clinopyroxene is fresh, and hornblende is altered (Item S7E).

Thin scoriaceous basaltic trachyandesite lavas rest conformably on the thick andesite lavas. They contrast with the thick andesite lavas by being much thinner and more vesicular and are capped by scoria lapilli rather than nonvesicular large blocks as in the *thick andesite lavas* (Items S6D-8 and S6D-9). They are also more mafic and phenocryst poor (sample SR 12-6, Table 1A).

The coherent interior of the Mina Victoria *trachyandesite lava dome* yielded a ^{40}Ar-^{39}Ar age of 13.81 ± 0.10 Ma (sample SR 12-4, Fig. 5). The experiment conducted with a groundmass concentrate yielded a plateau age of 13.90 ± 0.08 Ma for seven consecutive fractions representing more than 85% of the ^{39}Ar released (Fig. 8A-1). However, the isochron age of 13.81 ± 0.10 Ma (Fig. 8B-1) is taken as the best estimate because the data indicate that the $(^{40}Ar/^{36}Ar)_i$ is higher than the atmospheric value.

The Mina Victoria *thick andesite lavas* yielded an ^{40}Ar-^{39}Ar age of 10.1 ± 0.9 Ma (sample SR 12-2, Fig. 5). The sample came from the coherent interior of a lava in the middle of the section. ^{40}Ar-^{39}Ar experiments were performed with plagioclase and groundmass concentrates. The results of the groundmass and plagioclase are plotted together in the age spectrum and $^{36}Ar/^{40}Ar$ versus $^{39}Ar/^{40}Ar$ correlation diagram (Figs. 8A-4 and 8B-4). The results are characterized by low ^{40}Ar radiogenic (^{40}Ar*). The age spectra for the groundmass concentrate indicate severe argon loss that reaches a small plateau segment defined by three fractions with the highest ^{40}Ar* (Fig. 8A-4). Their weighted mean yields a 12.12 ± 0.51 Ma age. The best age estimate of sample SR 12-2 is the plateau age of 10.1 ± 0.9 Ma obtained with all the fractions of the plagioclase step-heating experiment.

Sawlan and Smith (1984) reported K/Ar ages on a sample that plots within our *thick andesite lavas* (sample 82BSJ104B, Fig. 3B), when we apply the coordinates reported in their paper, and an air photo with a plotted sample location, as kindly provided to us by Michael Sawlan (2019, written commun.). The sample came from a dike, and XRF geochemistry indicates it is an andesite (Sawlan, 2019, written commun.; see geochemical data in Item S2 [footnote 1]). Because only six trace elements were analyzed for this sample, we were not able to confidently determine whether the dike is calcalkaline or rift transitional in chemistry. Sawlan and Smith (1984) reported duplicate whole-rock ages on that sample, of 12.3 ± 0.4 Ma and 12.5 ± 0.4 Ma. This K/Ar age appears to be too old since this dike is within the *thick andesite lavas* that we date at 10.1 ± 0.9 Ma.

We did not sample the *thin scoriaceous basaltic trachyandesite lavas* map unit for geochronology because it is very altered due to its scoriaceous nature.

East of Curuglu Fault

We mapped two units in the area along the east side of the Curuglu fault (Fig. 3); both units are calcalkaline (Table 1A). These are described in stratigraphic order.

Basaltic andesite to andesite tuff of Curuglu is a mafic ignimbrite that is >25 m thick, with its base truncated by the Curuglu fault. In outcrop, it is a pink scoria lapilli tuff (Item S6E-1 [footnote 1]), and in thin section, vitroclastic texture is obvious, including brown relict glass with microlites, vesicles, and bubble-wall shards (Item S7F). This mafic ignimbrite is divided into internally massive beds, or flow units, 8–10 m thick, with sharp contacts. The basal flow unit has abundant black to dark-gray aphyric angular blocks that are andesite (sample SR 08-1, Table 1A, Item S6E-1 [footnote 1]). The second flow unit lacks lithics; a whole-rock sample of this has abundant crystals of plagioclase and clinopyroxene and is basaltic andesite (sample SR 08-2, Table 1A, Items S2 and S7F). The second flow unit is density graded, with scoria block concentrations at its top (Item S6E-2). A single one of these scoria blocks was sampled, and it is an aphyric andesite (sample SR 08-3, Table 1A, Item S2). This suggests that the matrix underwent a high degree of crystal enrichment during eruption and transport. The second flow unit is capped by 35-cm-thick, well-sorted lapillistone (Item S6E-2), which records fluvial working before deposition of the third flow unit, which also lacks lithics. Locally, a 10-m-deep channel is incised into the top of the tuff of Curuglu, filled with crudely stratified volcanic lithic breccia-conglomerate and pebbly sandstone, interpreted as fluvial and debris flow deposits (Item S6E-3). The *basaltic andesite to andesite tuff of Curuglu* is now covered by the tailings pond for the mine.

Mafic ignimbrites (i.e., andesite or basaltic andesite scoria-rich pyroclastic flow deposits) are unusual, but they do occur in arc settings (e.g., Fisher and Schmincke, 1984; Freundt et al., 2000; McCurry and Schmidt, 2001; Busby and Bassett, 2007). They are very small in volume and therefore are not deposited far from the vent. This fact and the presence of block-sized andesite clasts in the *basaltic andesite to andesite tuff of Curuglu* indicate that this is a vent-proximal mafic ignimbrite. The tuff of Curuglu is conformably overlain by andesite lava.

The *andesite lava* map unit is a single, 22-m-thick hornblende clinopyroxene andesite lava (sample SR 08-4, Table 1A, Item S2). It is dominated by flow breccia (Item S6E-4), with <20% coherent flow interior. The groundmass and plagioclase are fresh, and the hornblende is altered (Item S7G [footnote 1]).

The geochronology sample from the *andesite lava* map unit (SR 08-4, Fig. 5) was taken as far away from the Curuglu fault as possible (~100 m), to avoid alteration. Two experiments were performed on a groundmass concentrate and yielded reproducible results. The plateau age of 11.50 ± 0.18 Ma was calculated with the weighted mean of seven consecutive fractions that represent 84.36% of the ^{39}Ar released (Fig. 8A-5). The combined data for the two experiments define a slightly younger isochron age because the (^{40}Ar/^{36}Ar)$_i$ is higher than the atmospheric value (Fig. 8B-5). Therefore, the isochron age of 10.83 ± 0.95 Ma is taken as the best age estimate for sample SR 08-4 (Fig. 5 and Table 1A).

El Morro

The El Morro area (Fig. 3) has outstanding sea cliff and arroyo exposures of ignimbrite referred to by Conly et al. (2005) as the El Morro Tuff, and informally referred to herein as the tuff of El Morro. It is a trachydacite to rhyolite nonwelded to welded ignimbrite and is the oldest map unit that we assign to the rift transitional geochemical group (Table 1A; Fig. 5; Item S2), discussed below. We summarize key features of this ignimbrite herein, and we provide more detailed outcrop and petrographic descriptions in the Supplemental Items (Items S6F-1–S6F-10 and S7H–S7K), in hopes that it will be recognized elsewhere and used as a stratigraphic marker. Only 50 m of the tuff of El Morro is exposed, with the base covered and the top eroded and locally overlain by Boleo Formation sedimentary rocks. We have divided out three map units within the tuff of El Morro (Fig. 3): *pink nonwelded lithic rhyolite to trachydacite ignimbrite, purple welded rhyolite ignimbrite,* and *basaltic trachyandesite lavas interstratified with pink nonwelded lithic ignimbrite* (Table 1A).

The *pink nonwelded lithic rhyolite to trachydacite ignimbrite* dominates the tuff of El Morro and is massive nonwelded ignimbrite (in exposures tens of meters thick) that is weakly welded in intervals where lithics are less abundant (Fig. 7A; Items S6F-1 and S7H–S7I). The *purple welded rhyolite ignimbrite* consists of lithic-free intervals that are densely welded (Fig. 7B; Items S6F-3, S6F-4, and S7K). The tuff of El Morro is nearly aphyric, with <1% plagioclase in the pumices and <5% plagioclase in the matrix. We analyzed a single pumice block and it is trachydacite in composition (sample SR 15- 6, Table 1A, Item S2 [footnote 1]). Whole-rock samples of *pink nonwelded lithic rhyolite to trachydacite ignimbrite* (which vary in lithic content) are rhyolite to trachydacite in composition (Table 1A). The lithic fragments are mainly angular clasts of the *purple welded rhyolite ignimbrite* (Item S6F-8); these clasts also occur sparsely in the *purple welded rhyolite ignimbrite* (Item S7K). One of these *purple welded rhyolite ignimbrite* clasts was sampled and is petrographically and chemically identical to the *purple welded rhyolite ignimbrite* where it forms an in situ sheet (Table 1A). Additionally, the *pink nonwelded lithic rhyolite to trachydacite ignimbrite* has lenses within it that consist of boulders of pink weakly welded ignimbrite, which are identical to the *pink nonwelded lithic rhyolite to trachydacite ignimbrite,* where it forms in situ sheets (Item S6F-7). These boulders, in turn, contain lithic fragments of the *purple welded rhyolite ignimbrite* (Item S6F-9). These relations indicate repeated cannibalization. This is typical of caldera fill, where earlier-erupted ignimbrite that welds on the walls of a caldera, or onto intracaldera blocks that collapse piecemeal, gets broken up and redeposited into the caldera during later stages of eruption and caldera collapse (Lambert, 1974; Lipman, 1976; Branney and Kokelaar, 1994; Schermer and Busby, 1994).

Along the sea cliffs on the east side of the Santa Agueda estuary (Fig. 3), the *pink nonwelded lithic rhyolite to trachydacite ignimbrite* is cut by large-scale blocky injection structures. These form clastic sills and dikes that are very irregular in shape and orientation (Items S6F-5 and S6F-6). The blocks are solely *purple welded rhyolite ignimbrite*, indicating that the injection structures formed before any younger units were deposited (for example, the *basalt lava* and the *basaltic andesite lava* at Cerro Juanita, Figs. 3 and 5). We interpret these injection structures to record landsliding soon after the purple and pink ignimbrites were deposited, either on an active fault block or in a subsiding caldera.

The *pink nonwelded lithic rhyolite to trachydacite ignimbrite* has two interstratified *basaltic trachyandesite lavas*, mapped separately (Fig. 3 and Table 1A). The ignimbrite that encloses them is massive, with no evidence of fluvial reworking;

therefore, we infer that little time is represented for deposition of the tuff of El Morro, despite the presence of interstratified lavas. A white pumice block concentration is partially admixed with the uppermost part of the flow-top breccia on the upper lava (Items S6-F1 and S6-F2 [footnote 1]). This may be similar to lee-side coarse pumice lenses in the Taupo ignimbrite, which are found in the lee of topographic obstacles (Walker and Wilson, 1983), which the lava evidently formed.

We did not sample the tuff of El Morro ignimbrite for ^{40}Ar-^{39}Ar geochronology because it is too altered. Conly et al. (2005) referred to the tuff of El Morro as "conglomeratic tuff" (presumably lithic ignimbrite) and obtained a range of K-Ar ages on "clast separates" (indicating volcanic lithics?) of 11.71Ma ± 0.62–8.62 ± 0.21 Ma, and on matrix, overlapping ages of 8.94 ± 0.80–8.22 ± 0.39 Ma. The groundmass of the interstratified basaltic trachyandesite lavas is much fresher than the matrix in the enclosing tuff of El Morro ignimbrite (Item S7-J); so we dated the upper one of those two lavas by ^{40}Ar-^{39}Ar.

The *basaltic trachyandesite lava* sample SR 15-8 yielded reproducible results and well-defined plateau segments in the two experiments performed on groundmass. The plateau age of 9.75 ± 0.14 Ma, calculated with five consecutive fractions representing 76.6% of the ^{39}Ar released, is statistically indistinguishable from the isochron age of 9.69 ± 0.12 Ma calculated with the combined data of the two experiments (Fig. 8A-7). The isochron age of 9.69 ± 0.12 (Fig. 8B-7) is taken as the best estimate for the age of the *basaltic trachyandesite lava* (Fig. 5), as well as the ignimbrite (tuff of El Morro) that encloses it. This is older than the age Conly et al. (2005) obtained on matrix from his "El Morro Tuff," likely because the ignimbrite matrix is altered.

In addition, we chiseled out several kg of pumice blocks from the white pumice block concentration described above (sample SR 15-6, Table 1), and we separated the pumice blocks for zircons (Fig. 9). The yield was small, probably because the pumices are nearly aphyric (sample SR 15-6, Table 1). U-Pb analyses were conducted on the CAMECA IMS 1270 ion microprobe at University of California, Los Angeles (Items S1 and S4 [footnote 1]). The sample included two concordant antecrysts (21.19 Ma ± 0.92 and 12.63 Ma ± 1.08; 1σ uncertainty) and two anomalously young grains with low radiogenic ^{206}Pb; these two grains were excluded from the mean age determinations. The sample yielded a concordant mean weighted $^{206}Pb/^{238}U$ age of 9.00 Ma ± 0.2 (2σ) based on 11 grains (Fig. 9A) in excellent agreement with the Tera-Wasserburg concordia age of 9.04 Ma ± 0.14 (2σ; Fig. 9B). This is slightly younger than the ^{40}Ar-^{39}Ar age on the interstratified lava, perhaps due to differences in techniques and sample types. More interesting is the result from the Hf isotope work (Fig. 9C), described below in Geochemistry.

Arroyo Purgatorio

The Arroyo Purgatorio area is mapped as one unit, *basaltic andesite lava,* which we designate as rift transitional in chemistry (Fig. 3A, Table 1A, Item S2 [footnote 1]). It is clearly extrusive because it has flow-top and flow-bottom breccias. In addition, we sampled a body that is too small to map individually; therefore, it is included in the *basaltic andesite lava* map unit (Fig. 4A). This body is a coherent clinopyroxene dacite that may either represent a lava or an intrusion and is calcalkaline (Table 1A, Item S2). The rocks in this area are highly faulted and

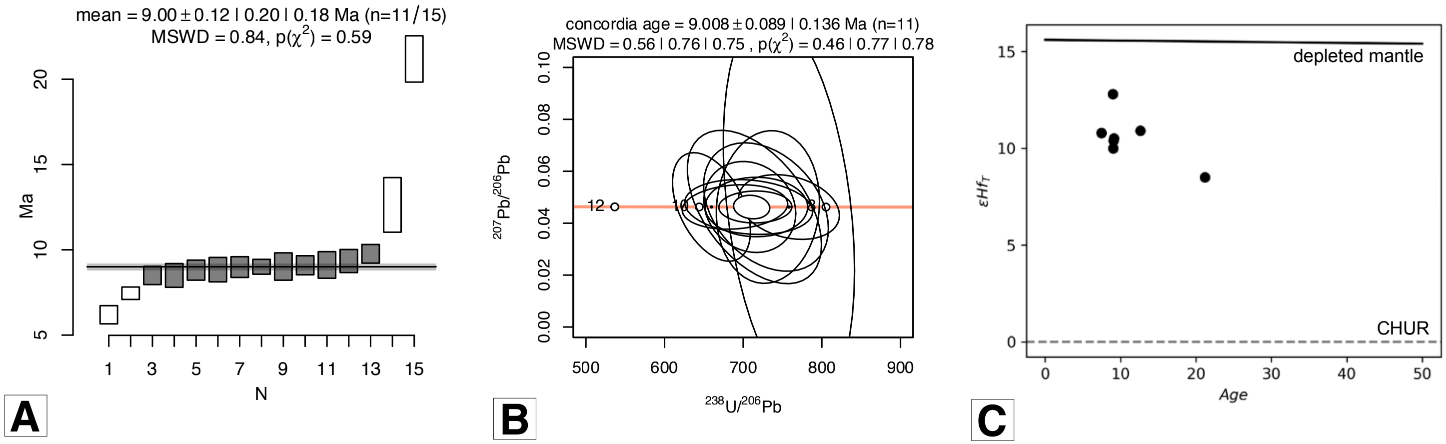

Figure 9. Zircon analyses from pumices extracted from tuff of El Morro (sample SR15-6, Table 1). Methodology and data tables for U-Pb zircon geochronology and Lu-Hf isotopic analysis provided in Supplemental Items (Items S6–S8) (text footnote 1). (A) Ranked $^{206}Pb/^{238}U$ age distribution. Weighted-mean age of 11 of 15 concordant individual zircon grains is 9.00 Ma ± 0.2 (2σ), mean standard weighted deviation = 0.84. (B) Tera-Wasserburg concordia plot of 11 zircon grains. Concordia age of 9.04 Ma ± 0.14 (2σ), mean standard weighted deviation = 0.74. (C) εHf_T plot. Chondritic uniform reservoir (CHUR) = $^{176}Lu/^{177}Hf$ = 0.0336 ± 1 and $^{176}Hf/^{177}Hf$ = 0.282785 (Bouvier et al., 2008). The high positive εHf_T values are consistent with magma genesis in the rift transition (see text).

altered; thus, stratigraphic and intrusive relations are unclear, and no samples were dated.

Cerro Juanita

The Cerro Juanita area has two map units: *basalt lava* and an overlying b*asaltic andesite lava* (Fig. 3, Item S2), and we designate both as rift transitional in chemistry (Table 1A).

Basalt lava consists of a single, ~30-m-thick, plagioclase-rich lava (Table 1A, Item S6G). This lava lacks basal and upper flow breccia and rests on purple, thin-bedded tuff and lapilli tuff. The thickness of this basalt is suggestive of ponding in a graben.

Basaltic andesite lava forms a single lava that is >100 m thick, with a basal flow breccia (Item SG) and its top eroded. The upper preserved part, which was quarried to build the harbor at Santa Rosalía, is more aphyric than the lower part (Table 1A). Therefore, there may be more than one flow unit, although the chemistry is the same, and there are no intervening flow breccias or scoriaceous horizons. If it is one flow, its thickness may indicate ponding in a graben.

The phenocryst-poor part of the *basaltic andesite lava* was the freshest (Item S7L), so it was chosen for geochronology (sample SR 14-1). The data from two experiments yield reproducible results and very well defined plateau segments (Fig. 8A-8). The plateau age of 9.66 ± 0.21 was calculated with the weighted mean of six consecutive fractions that represent 73.41% of the ^{39}Ar released. The plateau age is statistically identical to the isochron age (9.71 ± 0.34 Ma) calculated with the combined data of the two experiments (Fig. 8B-8). The more precise plateau age of 9.66 ± 0.21 is taken as the best estimate for the *basaltic andesite lava* of Cerro Juanita (Fig. 5).

Cerro Sombrero Montado

The Cerro Sombrero Montado area has two map units—*lithic pumice lapilli tuff* and an overlying *andesite lava* that we designate as rift transitional in chemistry (Fig. 3; Table 1A; Item S2 [footnote 1]). These units dip east (Item S6H), as do the nearby lavas on Cerro Juanita (Fig. 3), but the *andesite lava* that caps Cerro Sombrero Montado is younger than the *basaltic andesite lava* on Cerro Juanita (Fig. 5). Like the section on Cerro Juanita, the base of the section at Cerro Sombrero Montado is a pyroclastic rock (*lithic pumice lapilli tuff,* Fig. 3).

Lithic pumice lapilli tuff. The basal deposit on Cerro Sombrero Montado consists mostly of pumice lapilli and smaller pumice shreds, with ~20% euhedral or broken crystals and 20% volcanic rock fragments (Table 1A). We did not analyze it for geochemistry because of the abundant volcanic rock fragments (Item S7M). It is exposed directly beneath the overlying, resistant andesite lava, for a thickness of ~10 m. This is the only hornblende tuff we have found. The predominance of pumice lapilli in the deposit is suggestive of Plinian fall, and if it is a fall deposit, its thickness and the presence of lithics may indicate it is proximal to the vent.

Andesite lava. This map unit consists of a single phenocryst-poor lava >80 m thick (top eroded, Fig. 3), with a basal flow breccia (Table 1A). It has <5% plagioclase phenocrysts, most skeletal or sieve textured, and plagioclase microlites with interstitial clinopyroxene (Item S7N).

The two experiments performed with whole-rock sample SR 14-5 (*andesite lava*) yielded age spectra with some perturbation. However, a very good plateau age of 8.84 ± 0.16 Ma was obtained from the weighted mean of seven consecutive fractions that represent 87.27% of the ^{39}Ar released (Fig. 8A-9). The distribution of the combined data of the two experiments does not constrain the straight line on the (^{36}Ar/^{40}Ar) versus (^{39}Ar/^{40}Ar) correlation diagram (Fig. 8B-9); for this reason, the plateau age is taken as the best estimate for the age of sample SR 14-5 (Fig. 5).

Santa Rosalía South

The Santa Rosalía south area is a contiguous map area dominated by two main map groups: calcalkaline volcanic and volcaniclastic rocks and high-magnesian andesite (Fig. 4; Table 1B). Each of these two main groups is subdivided into map units (Fig. 4), some of which interfinger or repeat. The high-magnesian andesite lavas clearly overlie the calcalkaline lavas, and the high-magnesian andesite intrusion clearly crosscuts the calcalkaline lavas (Fig. 4).

Calcalkaline volcanic and volcaniclastic rocks. Volcanic lithic *fluvial sandstones* and *volcanic debris flow deposits* and *undifferentiated sedimentary rocks* form the base of the section (Fig. 4). We found no primary volcanic rocks to date in this section. Andesitic volcanic lithic sandstones and conglomerates from the Loreto area southward (Fig. 1) occur in the Lower Member of the Comondú Group (ca. 24–19 Ma; Umhoefer et al., 2001; Drake et al., 2017); however, Loreto is nearly 200 km to the south, and the Comondú Group in the intervening area is poorly known. Furthermore, volcanic fluvial sandstones lie in the "East of Curuglu Fault" section, described above, and intervals of volcanic fluvial sandstone are common in arcs. However, if these sandstones are indeed Lower Member of the Comondú Group, this would indicate that there is a ~10 m.y. unconformity between the basal sedimentary rocks and the *andesite lavas* above.

The section of *andesite lavas* has a relatively continuous *red hornblende andesite lava* and a lens of *dacite block-and-ash-flow tuff* (Fig. 4). The andesite lavas were not mapped individually but generally dip eastward. The *andesite lavas* map unit is ~200 m thick, and the lavas are all very similar in appearance: dark-colored, with thick flow breccias, and commonly flow banded. All have clinopyroxene and no hornblende (Item S7O [footnote 1]), except for the *red hornblende andesite lava* (Fig. 4), which has hornblende and no pyroxene (Table 1B). Like the *andesite lavas,* the *andesite block-and-ash-flow tuff* in the southeast part of the map has abundant clinopyroxene and no hornblende (Item S7P); thus it probably records flow-front collapse of *andesite lava*. The *dacite block-and-ash-flow tuff* within the *andesite lava* section (Fig. 4 and Table 1B) forms a 15-m-thick lens that is visible from the dirt road in the arroyo ~1 km to the west, because its light-gray color contrasts with the dark color of the andesite lavas above and below, and it weathers recessively. It forms a deposit of angular blocks in a matrix of lapilli and ash of the same composition (Item

S6I-1 [footnote 1]). It has abundant plagioclase phenocrysts and lesser hornblende, largely replaced by opaque minerals (Item S7Q). This is the only silicic volcanic unit we have found in the Santa Rosalía south map area (Fig. 4).

Groundmass sample SL 08-4 was prepared from the calcalkaline *andesite lava*. Two experiments were performed with reproducible and well-defined broad plateau segments. The plateau age of 10.48 ± 0.09 Ma was obtained with eight consecutive fractions that represent 85.03% of the ^{39}Ar released (Fig. 8A-6). The combined data of the two experiments are well aligned in the (^{36}Ar/^{40}Ar) versus (^{39}Ar/^{40}Ar) correlation diagram defining an isochron age of 10.11 ± 0.14 Ma (Fig. 8B-6); that age is taken as the best estimate for the age of *andesite lava* sample SL 08-4 (Fig. 5).

High-magnesian andesite. This includes *trachyandesite lavas* and *trachyandesite intrusions* (Fig. 4). East-dipping, high-magnesian *trachyandesite lavas* overlie the calcalkaline *andesite lavas* as well as the *undifferentiated sedimentary rocks* on the east flank of Cerro San Lucas, in angular unconformity (samples SL 08-5 and SL 08-7, Fig. 4 and Table 1B). Flow breccias 2–4 m thick (Fig. S6I-2) alternate with coherent interiors of similar thickness. These lavas differ from the calcalkaline *andesite lavas* by having hornblende as well as clinopyroxene phenocrysts, although the hornblende is commonly pseudomorphed by opaque minerals (Item S7R [footnote 1]). The hornblende in the high-magnesian *trachyandesite intrusions* (Table 1B) is generally much better preserved, and large (~2 mm), with fine oscillatory zoning (Fig. 7C). These hornblendes are similar in appearance to those of the 1991–1995 Unzen dacite, Japan, which have finely alternating Fe-rich and Mg-rich zones detected by electron microprobe (Sato et al., 2005). That zoning was interpreted to be the result of repeated convective degassing and fluid recharge of the magma. The small high-magnesian *trachyandesite intrusion* on the west end of the map area intrudes volcanic debris flow deposits of uncertain age, but the larger high-magnesian *trachyandesite intrusion* clearly crosscuts the calcalkaline *andesite lavas,* forming the highest peak in the Cerro San Lucas, with a radio tower on top (note that the road to the tower is not always passable by 4WD). Both plugs represent hypabyssal intrusions, with hornblende ± clinopyroxene phenocrysts set in a groundmass of plagioclase microlites and no plagioclase phenocrysts (Table 1B). The larger *trachyandesite intrusion* is very well exposed along the road to the tower and has miarolitic cavities (Fig. 6F). These cavities commonly occur in shallow-level granites or pegmatites but may also occur in hypabyssal intrusions (Kiddle et al., 2010), providing evidence of a potentially fertile intrusion (Harris et al., 2004).

A hornblende and a groundmass concentrate were analyzed from the larger clinopyroxene hornblende high-magnesian *trachyandesite intrusion* (sample SL 08-1), collected near the top of the intrusion (Fig. 4). The age for this sample is 6.06 ± 0.27 Ma (Fig. 5). This age is the weighted mean of two fractions of the experiment performed with the hornblende concentrate (Fig. 8A-10); these fractions represent 74% of the ^{39}Ar released. This age is in agreement within 1σ errors to the weighted mean age (5.92 ± 0.29 Ma) of three consecutive fractions of the experiment performed with the groundmass concentrate and with the isochron age of 6.01 ± 0.86 Ma (Fig. 8B-10) calculated with the fractions released at high temperature of the hornblende and groundmass experiments.

GEOCHEMISTRY

Cenozoic volcanic rocks on the Baja California Peninsula have been divided into geochemical groups based on whole-rock major- and trace-element characteristics. Previously recognized geochemical groups include calcalkaline, adakite, high-magnesian andesite (sometimes called bajaites), niobium-enriched basalt, and tholeiite lavas. The calcalkaline, high-magnesian andesite and adakite magmas reflect subduction-influenced melting or modification of mantle sources (Calmus et al., 2003; Conly et al., 2005; Negrete-Aranda and Cañón-Tapia, 2008).

In the Santa Rosalía area, whole-rock geochemistry shows a range of silica contents, with compositions 52–63 wt% SiO_2 dominating (Fig. 10A). Trace-element ratios (Figs. 10B–10D), including multi-element plots normalized to primitive mantle (Sun and McDonough, 1989) (Fig. 11), were used to divide samples into calcalkaline, rift-transitional, and high-magnesian andesite geochemical designations based on the relative abundances of light rare-earth elements and/or heavy rare-earth elements (LREEs/HREEs). These designations correlate temporally with the transition between subduction and rift tectonics (Fig. 5). No niobium-enriched basalts or tholeiites were identified in this or previous studies (Calmus et al., 2003; Conly et al., 2005) of the Santa Rosalía area.

The oldest volcanic rocks in the Santa Rosalía area (13.81–10.11 Ma, Fig. 5) are calcalkaline andesite, basaltic andesite, basaltic trachyandesite, trachyandesite, and dacite (Figs. 10 and 11). These occur in both the Santa Rosalía north (Fig. 4) and Santa Rosalía south (Fig. 5) areas. Calcalkaline chemistries are characterized by moderate alkali contents and enrichment in LREE (Fig. 11D). Subduction of the Farallon slab ceased by ca. 12.5 Ma, but two million years of postsubduction calcalkaline eruptive products are not unreasonable in a region that experienced ~12 million years of subduction magmatism. As noted above, residual arc signatures persisted for 4 m.y. in Sonora (Till et al., 2009), and calcalkaline volcanism recurred in the Quaternary at Tres Virgenes volcanic field (Fig. 2; Sawlan, 1991; Schmitt et al., 2006, 2010). Similarly, Putirka and Platt (2012) showed an up to 17 m.y. lag between the end of subduction and the disappearance of a subduction-related signal in the geochemistry of volcanic rocks in the Walker Lane–Sierra Nevada region of California.

A younger suite of volcanic rocks in the Santa Rosalía area (9.69–8.84 Ma, Fig. 5) shows greater enrichment of HREE relative to calcalkaline samples; the suite is herein designated rift transitional. These samples occur in the Santa Rosalía north area (Fig. 3). They include rhyolite to trachydacite ignimbrites, as well as basalt, basaltic andesite, andesite and trachyandesite lavas (Fig. 10). Although altered, the ignimbrite samples show higher HREE (Fig. 11C), and the rift transitional lavas have higher HREE and lower LREE, relative to calcalkaline rocks (Fig. 11B). This can be seen in the low La/Yb ratio of these lavas (Fig. 10D). The one exception is one of the two core samples through ignimbrite (tuff of El Morro, sample Montado-02, Table 1, Item S2), which has a distinctive peak in Sr (Fig. 11C) that is dissimilar to most rhyolites in the Baja California Peninsula (Ferrari et al., 2018). Because this peak is not associated with an abundance of plagioclase phenocrysts, the significance of this SR peak is not understood.

Five ca. 9 Ma zircon grains (U-Pb ages described above) yielded εHf_T values of +10–+12.8 (mean +10.9; Fig. 9C). The 12.63 Ma antecryst and a low ^{206}Pb grain (7.45 Ma ± 0.25 [1σ]) both yielded similar εHf_T values. The 21.19 Ma antecryst yielded a more evolved +8.5 εHf_T value. The εHf_T values suggest that the tuff of El Morro magma had a significant mantle component admixed to crustal material. The ca. 21 Ma antecryst is more evolved but also shows a significant mantle component. Regionally, adjacent ca. 20–25 Ma Sierra Madre Occidental (SMO) magmas have lower εHf_T values (+1 to +5); however, SMO ignimbrite flare-up magmas have between +5 and +8, coincident with greater mantle signature (~50%; Andrews et al., 2012). The high positive εHf_T values are consistent with magma genesis in the rift transition as primitive, mantle-derived melts ascended higher into the crust where they melted and then mixed with mid- and upper-crustal rocks having lower εHf_T. The Tuff of El Morro was not derived from the melting of crustal rocks.

The youngest suite of volcanic rocks in the Santa Rosalía area (6.06 ± 0.27 Ma, Fig. 5) consists of high-magnesian andesite lavas and intrusions (Fig. 10A and Table 1), which were found in the Santa Rosalía south area (Fig. 4). The high-magnesian andesites have higher abundances of K and Sr (Fig. 10C) and Ba and Nd relative to calcalkaline samples (Fig. 11A). Trace elements of these rocks (normalized to primitive mantle) display the steepest slope of all the geochemical designations, which can be represented by Sr/Y and La/Yb ratios (Figs. 10C and 10D). The high concentrations of Ba and Sr, relative to other incompatible elements such as Rb and Th, are distinctive (Fig. 11A; Calmus et al., 2003; Conly et al., 2005). The K/Rb ratios in the high-magnesian andesites are markedly higher

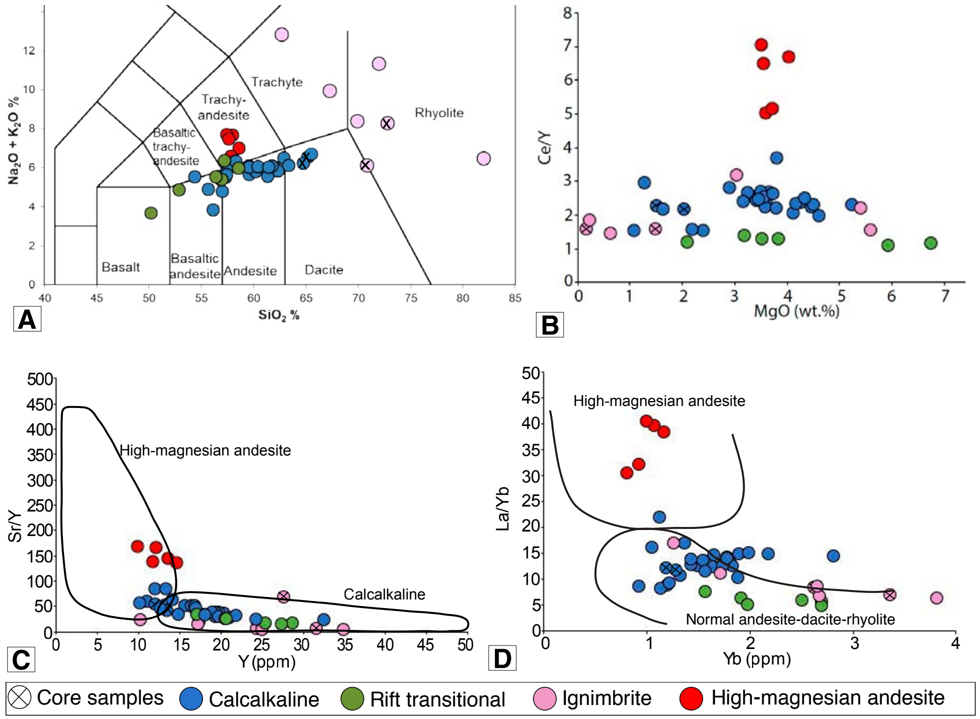

Figure 10. Geochemical plots of samples described in Table 1; data in Item S1 (text footnote 1). Samples were assigned to four groups: calcalkaline assemblage, rift transitional ignimbrites, rift transitional lavas, and high-magnesian andesite lavas and intrusions. Le Bas diagram (A) shows the diversity of bulk-rock chemistry. Trace-element ratios (B–D) highlight the distinctive character of the high-magnesian trachyandesites and the relatively depleted nature of the rift transitional lavas.

relative to the other chemical groups (up to 1400) and are comparable to K/Rb values of lavas in the Jaraguay and La Purisima volcanic fields (Rogers and Saunders, 1989; Sawlan, 1991).

There is some overlap in the geochemical characteristics of adakites and high-magnesian andesites, and both are recognized by high Sr/Y and La/Yb ratios, with adakites having lower ratios and higher silica contents (Richards and Kerrich, 2007; Moyen, 2009; Castillo, 2012; Item S8 [footnote 1]). Generally, high-magnesian andesite is a broader category, with higher ranges of observed Ba and Sr values than recognized in adakites (Item S8). We concur with Conly et al. (2005) that Cerro San Lucas rocks, which we date at 6.06 ± 0.27, are high-magnesian andesites.

High-magnesian andesites occur throughout central Baja California (Fig. 1), in the Jaraguay (3.00–10.3 Ma), San Borja (0.57–10.93 Ma), San Ignacio (3.08–5.07 Ma), La Purisima (1.01–9.67 Ma), and Vizcaíno (11.13 Ma) volcanic fields (Benoit et al., 2002; Calmus et al., 2003; Bellon et al., 2006; Pallares et al., 2007, 2008; Castillo, 2008; Negrete-Aranda and Cañón-Tapia, 2008; Negrete-Aranda et al., 2010, 2013; Calmus et al., 2011; Di Luccio et al., 2014). These high-magnesian andesites are all postsubduction in age. Adakites in central Baja California in the Santa Clara volcanic field (8.7–11 Ma; Aguillón-Robles et al., 2001) and in the Jaraguay volcanic field (9.4 Ma; Pallares et al., 2008) (Fig. 1) also postdate subduction. Some adakite-like compositions

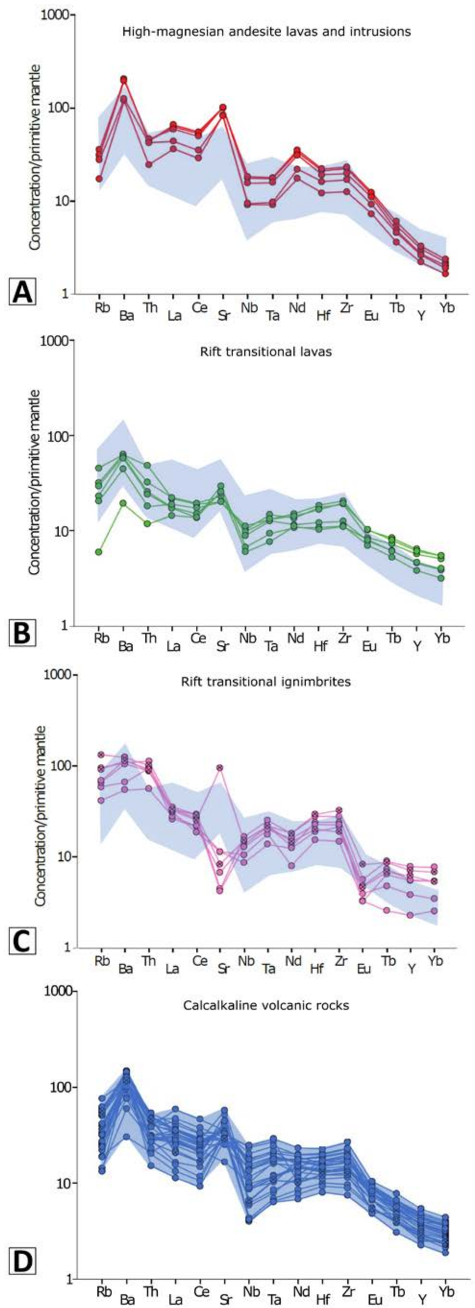

Figure 11. Multi-element plots of trace elements used to recognize the chemical groups (in stratigraphic order, from bottom to top): (D) calcalkaline, (C) rift transitional ignimbrite, (B) rift transitional lavas, and (A) high-magnesian andesite. The field of calcalkaline rocks is shown in each plot by blue shading. Rift transitional rocks (B and C) are less enriched in light rare-earth elements (LREEs) and more enriched in heavy rare-earth elements (HREEs) than calcalkaline rocks, and high-magnesian andesites (A) have exceptional enrichment in some incompatible elements, notably Sr and Ba, with distinctively low HREE abundances.

have been found at Tres Virgenes (ca. 100 ka; Sosa Ceballos et al., 2019). However, syn-subduction adakites are present in central Baja California at La Trinidad (LT, Fig. 1) (Busby et al., 2018b) as well as in mainland Mexico (Ferrari et al., 2018). The 5–6 Ma “adakites” of Bonini and Baldwin (1998) on Santa Margarita Island (SM, Fig. 1) may be more appropriately categorized as high-magnesian andesites, using the criteria given in Item S8 (footnote 1). Sr and Pb isotopic signatures of the high-magnesian andesites of Cerro San Lucas ($^{87}Sr/^{86}Sr$ 0.703723–0.704034; $^{206}Pb/^{204}Pb$ 18.43–18.61; Conly et al., 2005) are similar to other high-magnesian andesites elsewhere in Baja ($^{87}Sr/^{86}Sr$ 0.70355–0.7444, $^{206}Pb/^{204}Pb$ 18.64–18.764; Rogers and Saunders, 1989; and $^{87}Sr/^{86}Sr$ 0.70370–0.70399; $^{206}Pb/^{204}Pb$ 18.42–18.46; Negrete-Aranda and Cañón-Tapia, 2008).

Petrogenic models for high-magnesian andesites require a process in combination with source that preferentially concentrates LREE and Sr and Ba in magmas, producing high LREE and/or HREE but not similar enrichment of Rb and Th (Sawlan, 1991; Calmus et al., 2003). Proposed models include: (1) slab melting related to opening of an asthenospheric window (Calmus et al., 2003); (2) melting of metasomatized mantle (Sawlan, 1991; Conly et al., 2005; Calmus et al., 2011); and (3) crustal contamination (Richards and Kerrich, 2007). Melting of an amphibole-bearing metasomatized mantle source has been proposed to account for the high K/Rb (up to 3000) for high-magnesian andesites in Baja California (Rogers and Saunders, 1989; Sawlan, 1991; Calmus et al., 2011). Because amphibole does not host Rb and Th, this may explain the preferential concentration in melts of particular incompatible elements (Calmus et al., 2003). Although high Ce/Y ratios are frequently interpreted to suggest crustal contamination, the Ce/Y values of Santa Rosalía samples (Fig. 10B) exceed that of the regional crust, and Sr and Pb isotopic values do not support the interpretation of crustal contamination (Conly et al., 2005).

Geophysical evidence shows that there is currently a remnant slab beneath the central portion of Baja California, where the Guadalupe and Magdalena microplates lay offshore (Fig. 1; Wang et al., 2013; Di Luccio et al., 2014). This spatially correlates with high-magnesian andesites in Baja California (Fig. 1), which have all been produced since subduction ceased (<12.5 Ma; Calmus et al., 2003; Negrete-Aranda and Cañón-Tapia, 2008; Calmus et al., 2011). Negrete-Aranda and Cañón-Tapia (2008) suggest that it is unlikely that all the high-magnesian andesites across Baja California were formed from a single source but rather formed by localized processes due to spatial heterogeneities in postsubduction breakup of the slab, which has apparently spanned 12.5 Ma into the Holocene. For these reasons, we prefer the slab window hypothesis over the metasomatized mantle hypothesis for the high-magnesian andesites in the Santa Rosalía area, even though the petrologic data do not allow us to distinguish between them.

DISCUSSION

In this section, we discuss key stratigraphic, structural, intrusive, and geochronological relations for the Santa Rosalía area, shown in Figure 12, and place them in the larger context of the Guaymas basin and the plate margin (Fig. 1).

How Is the Arc-to-Rift Transition Recorded in Volcanic and Subvolcanic Intrusions in and around the Santa Rosalía Basin, and How Does This Compare to the Transition Elsewhere in the Gulf of California?

We used geochemistry to divide volcanic and intrusive rocks into a calcalkaline (subduction) assemblage, a rift transitional assemblage (subdivided into lavas and ignimbrites), and a high-magnesium andesite assemblage (subdivided into lavas and intrusions) (Fig. 12). In simple terms, relative to the subduction magmas, the rift transitional magmas show lower HREE and/or LREE ratios more similar to primitive mantle than typical subduction. ^{40}Ar-^{39}Ar geochronology was important to determine the ages of these geochemical suites and to determine if those ages were consistent with plate tectonic models for the timing of the arc-rift transition.

The arc-rift transition in the Santa Rosalía area forms a conformable stratigraphic section that spans ca. 14–9 Ma. The subduction phase was dominated by effusive volcanism, with explosive volcanism (tuff of El Morro) marking the onset of rift transitional volcanism (Fig. 12). Although subduction ceased by ca. 12.5 Ma, calcalkaline volcanism persisted until 10.11 ± 0.14 Ma here, and recurred in the Pleistocene at the Tres Vírgenes volcanic center, which overlies the Santa Rosalía basin fill on its north margin (Fig. 2). Volcanic rock compositions in the Walker Lane (the northward extension of the Gulf of California transtensional rift) show that continental mantle lithosphere with subduction signatures has taken up to ~20 m.y. to be completely degraded by asthenospheric upwelling due to rifting, with full asthenospheric compositions only appearing 20 m.y. after cessation of subduction, accomplished by northward passage of the Mendocino Triple Junction and opening of a slab window (Putirka and Platt, 2012; Putirka et al., 2012). This progressive degradation takes place in a piecemeal fashion at any one locality (see figure 16 of Putirka et al., 2012), resulting in mixed lithosphere-asthenosphere compositions of volcanic rocks and their included xenoliths. We refer to 9.69 ± 0.12 Ma to 8.84 ± 0.16 Ma rocks in the Santa Rosalía area as “rift transitional” because they record this process. However, the persistence of calcalkaline magmatism until 10.11 ± 0.14 Ma could alternatively be interpreted to record slow subduction of the Magdalena plate, interpreted by Michaud et al. (2006) to have occurred between ca. 12 and ca. 8 Ma.

Calcalkaline rocks in the Santa Rosalía area, and the Comondú arc of Baja California in general, are dominantly intermediate in composition and effusive, except for volcanic rocks of the Lower Comondú, which include Early Miocene silicic ignimbrites erupted in mainland Mexico (cf. Ferrari et al., 2018). Rift transitional rocks in the Santa Rosalía area, in contrast with the calcalkaline rocks, include basalt lava and silicic ignimbrite (tuff of El Morro). This is also true in the broader Gulf of California region. Basalts dated at 11.5–10 Ma extend 700 km along the coast of mainland Mexico (Ferrari et al., 2018). In the northern Gulf of California, rift silicic ignimbrites form two age groups. The older group, erupted at the initiation of rifting, includes (1) the tuff of San Felipe (Stock et al., 1999), dated at 12.50 ± 0.08 Ma (Bennett et al., 2013); (2) the tuff of San Ignacio, erupted synchronous with the tuff of San Felipe (Darin et al., 2016); and (3) the underlying Tuff of Cerro Colorado (Darin et al., 2016), which may also be rift related (its U-Pb zircon age, 14.20 ± 1.60 Ma, has large error). The second age

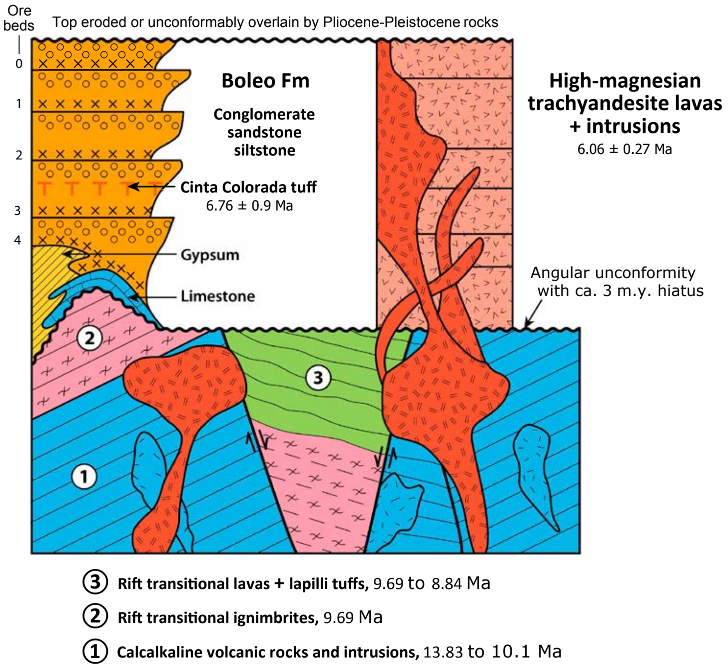

Figure 12. Schematic representation of stratigraphic, structural, intrusive, and geochronological relations described herein: Calcalkaline volcanic rocks (1) pass upward into rift transitional ignimbrites and lavas (2 and 3) with no time gap, and are transitional in chemistry as well as stratigraphy. These rocks were faulted and eroded prior to the onset of high-magnesian trachyandesite magmatism and deposition of the Boleo Formation. Marine limestone lies at the base of the Boleo Formation, locally overlain by gypsum deposits; these deposits in turn are overlain by coarsening-upward siltstone-sandstone conglomerate cycles. Cu-Co-Zn ore beds occur at the base of each cycle, probably because the basal siltstone formed a low-permeability barrier for fluids (Wilson and Rocha, 1955). The high-magnesian andesite intrusion is approximately the same age as the Boleo Formation (see text) and may have provided the heat engine and fluids for Boleo mineralization; alternatively, or in addition, the onset of seafloor spreading at ca. 6 Ma in the Guaymas basin could have provided the brines. Cinta Colorada tuff age from Holt et al. (2000); all other ages are from this study (Fig. 5).

group, at ca. 7–6 Ma, appears to correspond with the rapid development of pull-apart basins in the northern Gulf of California (Bennett et al., 2013). This includes seven rhyolite outflow ignimbrites at Puertecitos (^{40}Ar-^{39}Ar ages ranging from 6.7 to 6.1 Ma; Nagy et al., 1999), two outflow ignimbrites on Isla Tiburon (^{40}Ar-^{39}Ar ages of 6.44 ± 0.05 Ma and 6.01 ± 0.20 Ma; Bennett et al., 2015), as well as two airfall tuffs dated at 7.05 ± 0.03 Ma (^{40}Ar-^{39}Ar single crystal sanidine) and 6.53 ± 0.18 Ma (U-Pb zircon, sensitive high resolution ion microprobe–reverse geometry [SHRIMP-RG] spot analysis) by Bennett et al. (2013).

The tuff of El Morro ignimbrite marks the onset of rift transitional volcanism in the Santa Rosalía area, at 9.69 ± 0.12 Ma (Fig. 5), but it does not correspond in time with either the earlier rift initiation pulse or the later transtensional rift pulse in the northern Gulf of California. Furthermore, we have not been able to find reports of any ignimbrites of a similar age or description anywhere in the Gulf of California, and we have asked several active researchers if they know of any unpublished possibilities, and they do not. However, much of the large tract of volcanic rocks between Santa Rosalía and Loreto (Fig. 1) remains undivided; therefore, future work may identify correlative ignimbrites.

When Did Basin and Range–Gulf Extensional Province Extension Switch to the Transtensional Rift Regime at Santa Rosalía and in the Broader Gulf of California?

It remains unclear when the strain regime changed from orthogonal extension (Basin and Range–Gulf Extensional Province) to transtensional in the Gulf of California. In one model, early (ca. 12–6 Ma) strain was partitioned between NNW-trending dextral strike-slip faults west of the modern Baja California Peninsula (Fig. 1) and NNW-striking normal faults within the proto-gulf of California (Stock and Hodges, 1989; Oskin and Stock, 2003a, 2003b, 2003c; Oskin et al., 2001). In a second model, the strike-slip motion west of the Peninsula was small, and transtension dominated the Gulf of California beginning by 12 Ma (Fletcher et al., 2007; Bennett et al., 2013; Sutherland et al., 2012).

Umhoefer et al. (2018) argue that transtension had begun by ca. 7–8 Ma in the Gulf of California. If this is true, then the youngest volcanic rocks in the Santa Rosalía area (the 6.1 Ma high-magnesian trachyandesites, Fig. 12) must have formed under a regional transtensional regime. However, the tectonic setting of the rest of the volcanic rocks in the Santa Rosalía area (ca. 13.81–8.84 Ma, Figs. 5 and 12) remains unclear. A summary of regional relations is given here before addressing the Santa Rosalía area.

In the northern Gulf of California, normal faulting began at ca. 16–14 Ma on the Main Gulf Escarpment (Rossi et al., 2017), between ca. 16 and 11 Ma to the north of it in the Sierra Juarez (Lee et al., 1996), and at ca. 9–8 Ma to the east of it (Seiler et al., 2011, 2013). A pulse of detachment faulting occurred at ca. 10–15 Ma on the Monte Blanco dome, reactivated from Eocene time (Axen et al., 2000). Bennett et al. (2013, 2015, 2016, 2017) and Bennett and Oskin (2014) have shown that the northern 500 km of the 1500-km-long Gulf of California represented a zone of localized strike-slip faulting, clockwise block rotation, and subsiding pull-part basins from ca. 9–6 Ma, before marine incursion occurred at 6.2 Ma.

In the southern Gulf of California, Ferrari et al. (2013, 2018) infer that 11.5–10 Ma basalts along the eastern side of the Gulf of California were erupted on crust thinned by extension. Early Miocene (20.1–18.3 Ma) intermediate to silicic plutons within the southern Gulf of California are inferred to have been rapidly unroofed by extension (Duque-Trujillo et al., 2015). Other intrusions within the southern Gulf of California show evidence for unroofing at 10–9 Ma (Balestrieri et al., 2017). Drake et al. (2017) find no evidence of significant synvolcanic faulting in early to middle Miocene volcanic rocks on the Baja California Peninsula between Loreto and the north end of Bahía de La Paz (Fig. 1). However, south of La Paz, the high-angle San José del Cabo fault was active between 12 and 10 Ma (Fletcher et al., 2000) and is interpreted to be part of a transtensional shear zone (Fletcher et al., 2007). It had an earlier history as a detachment fault at ca. 17–12 Ma (Bot et al., 2016).

On a local scale, strain is commonly partitioned between normal faults and dextral faults in the Gulf of California as well as its northward extension, the Walker Lane (Axen et al., 2000; cf. Busby, 2013), making it difficult to demonstrate transtension without detailed mapping on a more regional scale than we present herein. Furthermore, it is difficult to demonstrate strike-slip displacement in the field, because piercing points can be difficult to find, and kinematic indicators are not commonly well developed in soft volcaniclastic rocks. It took a decade of mapping to determine that many central Sierra Nevada range front faults are oblique, not normal, and were produced by Walker Lane transtension, not Basin and Range extension (Busby et al., 2013a, 2013b, 2016, 2018a). Additionally, paleomagnetic work is needed to determine if dextral shear has been accommodated by vertical axis block rotations, as is observed in the central Walker Lane (Carlson et al., 2013; Carlson, 2017). In many cases, it is not known whether or not normal faults in the Gulf of California had a dextral component of slip (e.g., see discussion in Axen and Fletcher, 1998). Thus, it remains unclear when the transition from extension to transtension began in the Gulf of California and if the transition was synchronous or diachronous along the length of the Gulf.

On the basis of the mapping presented herein, we cannot determine if the subduction-related rocks were faulted during their accumulation. As stated above, we suspect that the rift-transitional lavas were deposited in extensional or transtensional basins because they are unusually thick. We also infer that the rift-transitional tuff of El Morro was disrupted by landslides prior to eruption of the rift transitional lavas, but that may have been triggered by caldera subsidence, rather than by extension or transtension, as described above. The subduction-related rocks and the rift transitional rocks were tilted and juxtaposed by faults and eroded prior to eruption of the 6.1 Ma high-magnesian trachyandesites and deposition of the Boleo Formation (Fig. 12), but there is too much Santa Rosalía sedimentary basin cover (Fig. 2) to be able to study those faults in detail. For this reason, we do not refer to these rocks as an "arc-oblique rift transition" but use the more general term "arc-rift transition." There are vast tracts of largely undivided volcanic rock in the ~300-km-long swath between the Santa

Rosalía area and the Loreto area (Fig. 1), and they must be studied in detail before we can fully understand the evolution of the Gulf of California rift.

How Does the Santa Rosalía Basin Stratigraphy Fit in with Regional Stratigraphic Models for Transtensional Rifting?

Umhoefer et al. (2018) presented a model for progressive seaway encroachment along en echelon pull-part basins in the Gulf of California. In their model, pre-rift rocks are overlain by nonmarine sedimentary rocks, in turn overlain by marginal marine evaporates, in turn overlain by marine rocks (presumably including limestones). However, this is the reverse of the stratigraphy in the Santa Rosalía basin (Fig. 12). It has long been known that marine limestone forms the base of the Boleo Formation (poorly constrained as late Miocene; Wilson and Rocha, 1955; Ortlieb and Colletta, 1984), and that these in turn are locally overlain by gypsum (Wilson and Rocha, 1955). Large positive values of $\delta^{34}S$ in the gypsum units (Ortlieb and Colletta, 1984) have been interpreted as evidence that they formed by evaporation of seawater in isolated basins (Ochoa-Landín et al., 2000). The overlying clastic rocks that dominate the basin fill (Fig. 12) consist largely of alluvial fan conglomerates and sandstones, although there are fine-grained sedimentary rocks interpreted as marginal marine tidal rhythmites (McCann et al., 2017). Thus, the Santa Rosalía basin does not fit the progressive seaway encroachment model of Umhoefer et al. (2018). Perhaps this is due to its unique setting adjacent to the Guaymas basin, which ruptured much earlier (by 3 Ma) than the rest of the basins in the Gulf of California.

Is There a Temporal Relationship between Slab Window Magmatism, the Onset of Guaymas Seafloor Spreading, and Boleo Cu-Zn-Co-Mn Mineralization in the Santa Rosalía Basin?

In this section, we present arguments that the Santa Rosalía basin may have formed and filled with Boleo Formation and its ore beds very quickly (ca. 100 ka), when seafloor spreading began in the Guaymas basin (ca. 6 Ma, Lizarralde et al., 2007) and when the high-magnesian trachyandesite intrusions were emplaced (6.06 ± 0.27 Ma, Fig. 12). This hypothesis is consistent with its position on the margin of the magma-rich Guaymas rift (Lizarralde et al., 2007), as well as its probable origin as a pull-apart basin (McCann et al., 2017). Attempts to constrain the age of the Boleo Formation include the following:

(1) The maximum depositional age of the Boleo Formation is constrained by the youngest volcanic rock we have dated that is overlain by Boleo Formation. This is the Cerro Sombrero Montado andesite lava (rift transitional), dated at 8.84 ± 0.16 Ma (Figs. 5 and 8). The contact is an angular unconformity, with the lava dipping 30° east beneath the Boleo Formation, which dips gently east (Figs. 3 and 12).

(2) The Boleo Formation has a single dateable tuff (Cinta Colorada, Fig. 12) that forms a decimeter- to 2-m-thick red marker bed in the northwest quadrant of the basin (Wilson and Rocha, 1955), covering an area of ~7.5 km^2 (Henry et al., 2015). It contains plagioclase crystals, andesitic volcanic rock fragments, and andesitic scoria, all altered, in a hematite cement. The location of its vent has not been found, but a small-volume mafic eruption is highly unlikely to provide an adequate heat source for the Cu-Zn-Co-Mn stratiform ore deposit as Conly et al. (2011) suggested it might. The ^{40}Ar-^{39}Ar date on the Cinta Colorada tuff reported by Holt et al. (2000) has large uncertainty (6.76 ± 0.90 Ma [2σ] isochron age). We think this is due to the alteration, based on examination of about a dozen thin sections from widely scattered localities. Preliminary paleomagnetic data (Holt et al., 2000) show that the Boleo Formation contains a geomagnetic polarity reversal (from normal to reversed), but there are seven of these in the 7.66–5.86 Ma interval allowed by the date on the Cinta Colorada (Holt et al., 2000). They used a series of assumptions to suggest an age of 7.1 Ma for the base of the Boleo Formation (Holt et al., 2000). This number is now widely used in the literature as "well constrained" (Miller and Lizarralde, 2013), but it is not. The base could be as young as 6.3 or 5.9 Ma (the age of the youngest two reversals that overlap with the age constraints on the Cinta Colorada). Furthermore, the sedimentation rate used by Holt et al. (2000) to calculate the age of the base is 280 m/m.y., which is normal for a rift basin but too slow for a pull-apart basin, which subsides and fills at over ten times that rate (Christie-Blick and Biddle, 1985; Pitman and Andrews, 1985; Ingersoll and Busby 1995; Nilsen and Sylvester 1995; Xie and Heller 2009; Allen and Allen, 2013). For example, the transtensional Loreto basin to the south by the town of Loreto (shown on Fig. 1) accommodated 615 m of fan delta sediments in only 100 k.y. (Dorsey et al., 1995).

(3) The Boleo Formation consists of monotonous andesitic volcanic lithic sandstone and conglomerate with minor siltstone (Ochoa-Landín et al., 2000; and our personal observations of dozens of thin sections made from samples taken at all stratigraphic levels). Although Wilson and Rocha (1955) describe the sandstones and siltstones as tuffs, there is no pyroclastic material (e.g., shards, pumice and/or scoria, or euhedral free crystals) in the Boleo Formation, and no evidence for contemporaneous eruptive products within the basin (e.g., block-and-ash-flow tuffs, pumiceous pyroclastic flow, or fall deposits) that might be suitable for dating. The only exceptions are the Cinta Colorada lapilli tuff, described above, and light-colored very fine-grained tuffs that lie above and below the Cinta Colorada in Arroyo de la Soledad on the western basin margin. We sampled the fine-grained light-colored tuffs and attempted to obtain zircon for dating, but the tuffs yielded none, perhaps because they are too distal. However, the possibility remains that ca. 7–6 Ma pulse of ignimbrite eruptions ~350–600 km to the north in the northern Gulf of California

(described above) delivered coarse, zircon-bearing fallout ashes to the Santa Rosalía Basin, and these ashes were resedimented rather than forming discrete layers of coarse-grained ash suitable for mineral separation for dating. Detrital zircon work was undertaken to test that possibility.

Sandstone samples weighing 88 kg each were collected from five stratigraphic levels, separated for detrital zircon, and analyzed for U-Pb ages by laser ablation–inductively coupled plasma mass spectrometry (LA-ICPMS) (Henry et al., 2017; Henry, 2019). Although ~315 zircons per sample were analyzed (out of a yield of ~1000 per sample), only 5–22 zircons per sample are <10 Ma, and of those, nearly all are >9 Ma, which does not improve existing depositional age constraints on the Boleo Formation (which overlies 8.84 Ma lavas in angular unconformity, as noted above). The poor yield of young zircons is consistent with the interpretation that the Boleo Formation was derived from erosion of andesite lavas and volcaniclastic rocks, which generally lack zircon. However, the youngest zircons are ca. 6 Ma in age (Henry, 2019), although these are very few and come from high in the section. This agrees well with our age on the high-magnesian andesite intrusions (6.06 ± 0.27 Ma, Fig. 5) and onset of spreading in the Guaymas basin (ca. 6 Ma, calculated from seafloor spreading rates; Lizarralde et al., 2007). The placement of laser pits in our zircons was generated by a program that guarantees representation of the overall detrital zircon population, which was dominated by 12–30 Ma and Cretaceous zircons (Henry, 2019). Future work will target euhedral zircons to see if we can determine the depositional ages of the base and top of the Boleo Formation.

(4) The sedimentology of the Boleo Formation suggests it may have accumulated in a very short time. Miller and Lizarralde (2013) infer that the 2 km of salt in the Guaymas basin could have been deposited in as few as ~57–115 k.y.; therefore, the 100-m-thick gypsum could have formed in an even shorter timespan. The clastic section is dominantly coarse grained and lacks paleosols or deep erosional unconformities or obvious angular unconformities. This suggests rapid subsidence and sedimentation. Its uniformly andesitic provenance and coarse-grained nature indicate a small drainage area undergoing uplift adjacent to the rapidly subsiding basin; although this occurs in orthogonal rift settings, it is more pronounced in strike-slip or oblique rift settings. The ore beds are associated with the fine-grained sedimentary rocks in the clastic section and are inferred to have formed from brine pools in a marginal marine environment, analogous to the Red Sea (Conly et al., 2006, 2011). These beds lack marine fossils entirely, probably due to a high rate of siliciclastic input, or presence of chemical toxins, or both (McCann et al., 2017).

If the Boleo Formation did indeed take <~100 k.y. to accumulate, the high-magnesian trachyandesite hypabyssal intrusions could have contributed to the heat source and fluids. The high-magnesian trachyandesite hypabyssal intrusions we mapped (Fig. 4) are too small to provide heat and fluids for a timespan of 100 k.y., but they may only represent cupolas on the top of a much larger intrusion that underlies the basin, and that is a reasonable time span for cooling of a larger intrusion. High-magnesian andesites and adakites are associated with Cu porphyry deposits in Japan and the Philippines (Richards and Kerrich, 2007; Castillo 2012), suggesting that these magmas are fertile. This is consistent with the presence of miarolitic cavities in the high-magnesian trachyandesite intrusion, described above (Fig. 6F), which also provides evidence of fertile intrusions (Kiddle et al., 2010). This is also consistent with the presence of finely alternating zones in its hornblende (Fig. 7C), which may be the result of repeated convective degassing and fluid recharge of the magma, by analogy with Unzen volcano (Sato et al., 2005). We therefore tentatively propose that the high-magnesian trachyandesite intrusions exposed along the southern margin of the Santa Rosalía basin may have provided the heat and fluids for coeval sedimentary stratiform Cu-Co-Zn-Mn Boleo mineralization (Fig. 12).

Alternatively, the heat engine and fluids may have been provided by the onset of seafloor spreading in the adjacent Guaymas basin at 6 Ma. It is not possible to separate the heating that the high-magnesian andesite intrusions may have provided from a regional source such as the onset of rifting in the Guaymas basin because they are coeval. In rifts, evaporites typically form under conditions unique to the latest stages of continental rupture and the onset of seafloor spreading (Evans, 1978; Miller and Lizarralde, 2013). If the Boleo Formation accumulated very rapidly, as discussed above, then the ore beds may have formed at the onset of seafloor spreading in the magma-rich Guaymas basin.

What Does the Magmatic and Structural Evolution of the Santa Rosalía Area Tell Us about the Origin of the Guaymas Basin?

The Guaymas basin is a narrow rift segment (terminology of Hopper and Buck, 1996) that has been robustly magmatic since continental breakup (Lizarralde et al., 2007). Magmatism in the Guaymas basin is anomalous, with ~8 km of igneous product, compared to mid-ocean ridge production (6 km) of basins to the south in the Gulf of California. Lizarralde et al. (2007) pointed out that magmatic activity in the Gulf of California varied over smaller length scales than could be explained by variations in extension rate or mantle temperature and heat flow. They instead suggested that mantle fertility controlled areas of robust rift and postrift magmatism, and that this may be related to the pre-rift magmatic history. They proposed that the mantle became depleted by Miocene ignimbrite volcanism in the southern Gulf of California. Our onshore data show that subduction-related magmatism continued until ca. 10 Ma in the Guaymas basin; so this may have contributed to mantle fertility and/or hydration.

Miller and Lizarralde (2013) considered evaporites to represent "the first deposition in proto-gulf extensional basins" (p. 285); however, we show here that rift transitional lavas (first identified by Conly, 2005) were likely ponded in extensional basins, and that rift transitional lavas and ignimbrites were juxtaposed against calcalkaline lavas by extension prior to deposition of the Boleo Formation evaporites (Fig. 12). Heat supplied by rift-related magmatism aids in evaporation from brines in the Afar triangle (Orszag-Sperber et al., 1998; Jackson and Cramez, 2000), as may have been the case during magma-rich rifting of the Guaymas basin (Lizarralde et al., 2007), and its onshore equivalent, the Santa Rosalía basin. The "igneous basement" below the east Guaymas evaporite is inferred from seismic properties to consist of extended continental crust with rift-related magmatic intrusions (Lizarralde et al., 2007; Miller and Lizarralde, 2013). By analogy with the Santa Rosalía area, some of the rocks there are likely calcalkaline lavas of the Comondú arc.

Nearly all of the volcanic rocks in the Santa Rosalía area dip eastward (Figs. 3 and 4). These rocks are clearly tilted, as shown by the attitudes of interstratified sandstones and tuffs, as well as ignimbrite compaction fabrics. Eastward tilting of the ca. 14–9 Ma volcanic rocks may have been accomplished by normal slip on a fault that now lies below sea level offshore. This is consistent with the fact that the shape of the east Guaymas evaporite indicates that the basin it formed in was bounded by N-S normal faults, which were active before the onset of northwest-southeast transform faulting and seafloor spreading at a northeast-southwest ridge (Miller and Lizarralde, 2013).

Speculation: Could a Slab Tear or Onset of Transtension Have Influenced High-Magnesian Andesite Magmatism in the Santa Rosalía Area and the Guaymas Basin?

The seismic structure beneath Baja California shows a distinct low-velocity (i.e., hot) zone crossing the Baja California Peninsula at ~28° North (Di Luccio et al., 2014), the latitude of the Santa Rosalía basin. We note that this lies above the boundary between the Guadalupe and Magdalena slab remnants (Fig. 1), and that the Di Luccio et al. (2014) image of the slab appears to bow out toward the paleotrench at this locality, suggesting that there is a slab window that crosses under the width of the Baja California Peninsula. The high-magnesian andesites in the Santa Rosalía area are further inboard from the trench than any others found so far in Baja California (Fig. 1). We speculate that this may possibly be explained by the presence of a large slab tear in this area. Perhaps this also contributed to the anomalously high magma production at the Guaymas spreading center and its early rifting relative to other basins in the Gulf of California. The high-magnesian andesites represent a pulse of trace-element–enriched magmatism at a time that broadly corresponds to the onset of transtension in the Guaymas rift. This may be similar to the onset of transtension in the western-central Walker Lane (the northern extension of the Gulf of California rift), where trace-element–enriched magmas were focused into a pull-apart basin (Putirka and Busby, 2007; Busby et al., 2018a).

CONCLUSIONS

We have used detailed field mapping, in conjunction with petrographic, geochemical, and ^{40}Ar-^{39}Ar geochronological analysis, to characterize the evolution of Miocene volcanic rocks surrounding the Santa Rosalía sedimentary rift basin of the Gulf of California, central Baja California Sur, México (Fig. 12). Our results also contribute to an understanding of the origin of the Guaymas oceanic rift basin, because the Santa Rosalía area represents the onland part of the Guaymas rift basin (Fig. 1).

Volcanic rocks in the Santa Rosalía area record the transition from calcalkaline subduction-related volcanism (13.81–10.11 Ma) to rift transitional volcanism (9.69–8.84 Ma). After an apparent volcanic hiatus of ~3 m.y., high-magnesian trachyandesite lavas and intrusions were emplaced at 6.06 Ma. Calcalkaline rocks consist of largely intermediate-composition lavas, block-and-ash-flow tuffs, and intrusions, with minor mafic ignimbrite and dacite. The onset of rift transitional volcanism is marked by eruption of the tuff of El Morro, a 9.69 Ma aphyric trachydacite to rhyolite ignimbrite that is nonwelded to weakly welded where it contains abundant lithics and strongly welded where lithics are absent. Repeated self-cannibalization of the welded to weakly welded ignimbrite during its eruption indicates remobilization of the earlier erupted ignimbrite from caldera walls or fault scarps. Landsliding immediately after emplacement of the tuff of El Morro also indicates remobilization due to tectonic activity or caldera subsidence. The age of the tuff of El Morro contrasts with the age of ignimbrites erupted at the onset of rifting elsewhere in the Gulf of California (ca. 12 Ma) and a second ignimbrite pulse at the onset of strong transtension (ca. 7–6 Ma). We have found no other reports of a 9.69 Ma ignimbrite in the Gulf of California or of an undated aphyric ignimbrite. Rift transitional lavas include basalt, basaltic trachyandesite, basaltic andesite, and andesite. Our mapping shows that nearly all of the volcanic rocks dip eastward, indicating they were rotated about an offshore fault, probably related to the N-S normal faults that ponded the east Guaymas evaporites.

Subduction-related calcalkaline rocks have the moderate alkali contents and high LREEs and low HREEs that are commonly associated with subduction. Postsubduction calcalkaline eruptions persisted for ~2 m.y. after subduction ceased, indicating that subduction-enriched mantle persisted in the area, typical of other arc-rift transitions, where degradation of such mantle lithosphere by rifting or opening of a slab window may take millions of years. Rift transitional rocks show more enrichment of HREE than the calcalkaline rocks, as well as less enrichment of LREE. Additionally, εHf_T data on zircons from the tuff of El Morro have a significant primitive (i.e., mantle) component admixed to more evolved, although still fairly primitive, crustal material. These data support the interpretation that the tuff of El Morro ignimbrite eruption marks the onset of rift transitional volcanism in the Santa Rosalía area.

The high-magnesian trachyandesites show incompatible element enrichment of K, Sr, Ba, and Nd. The trace-element abundances are depleted in HREE relative to the other groups and have high concentrations of Ba and Sr relative to Rb and Th. Melt generation was likely accomplished by a combination of slab melting related to opening of an asthenospheric window and melting of subduction metasomatized mantle. A remnant slab imaged beneath the central portion of Baja California spatially correlates with high-magnesian andesites. However, the high-magnesian trachyandesites in the Santa Rosalía area are the most inboard examples identified to date. We speculate that these were generated by a hot zone, imaged between the Guadalupe and Magdalena slab remnants, that extends eastward to the Gulf of California, which we interpret as a slab tear. We speculate that this hot zone may also have contributed to early rifting and anomalously high magma production at the Guaymas spreading center.

Sedimentary rocks of the Santa Rosalía basin overlie the eastward-tilted calcalkaline and rift transitional rocks in angular unconformity. The basin fill is dominated by the Boleo Formation, consisting largely of coarse-grained andesitic lithic sandstones and conglomerates, with basal limestone and gypsum, and with stratiform Cu-Co-Zn-Mn ore beds at several stratigraphic levels. The basal Boleo Formation gypsums formed on the margin of the Guaymas basin, where evaporates accumulated to a thickness of 2 km, probably in tens of thousands of years. Previous work has suggested that the ore beds were produced by brine pools. We present the preliminary interpretation that the Boleo Formation accumulated very rapidly (<100 ka) in a pull-part basin, coeval with the onset of seafloor spreading in the "magma-rich" Guaymas basin. This seafloor spreading may have provided the heat engine and fluids for mineralization in the Boleo Formation, perhaps aided by the emplacement of fertile high-magnesian andesite intrusions.

ACKNOWLEDGMENTS

This work was funded largely by the Baja Basins National Science Foundation (NSF) Research Experience for Undergraduates (REU) grant 151120 to principal investigator Tina Niemi and co-principal investigator Cathy Busby. Partial support from NSF grant EAR-1545676 (to Busby and Susan DeBari) is also gratefully acknowledged for providing some of the funds for geochronology and for supporting the participation of Busby's postdoctoral researcher, Sarah Medynski. A 2017–2018 UC Mexus-Conacyt Collaborative Research Grant (to Busby and López Martínez) funded the final stages of this work. This research was done over three years by REU mentors Busby, Graettinger, López Martínez, Medynski, and Niemi. The six undergraduate students and one M.S. student coauthor are listed in alphabetical order (Andrews, Bowman, Gutierrez, Henry, Lodes, Ojeda, and Rice). The undergraduate students participated for one year each, during their junior years, and the M.S. student (Henry) participated both as an undergraduate and as an M.S. student. The addresses of their undergraduate departmental homes are given here, to acknowledge these departments for giving these students the schedule flexibility needed to participate, and for the mentoring they provided before, during, and after their REU year. We thank the Minera Boleo for housing and feeding us and providing a classroom during the field work each January (2015–2017). Tina Niemi organized all of the logistics of the REU. We also thank Valente Salgado Muñoz, who facilitated our stay at the mine and access to outcrops and provided the drill-core samples of volcanic rocks. Thanks to Dr. Genaro Martinez Gutiérrez for his help with compiling and drafting the maps. We acknowledge the participation of CICESE's personnel, A. Susana Rosas Montoya and Gabriel Rendón Márquez for sample preparation, and Miguel Angel García García, who performed all the ^{40}Ar-^{39}Ar experiments.

Very helpful formal reviews by Paul Umhoefer and Michael Sawlan, and an informal review by Keith Putirka, are gratefully acknowledged. Discussions with Dan Lizarralde, Joann Stock, Luca Ferrari, Michael Oskin, and Marty Grove were also very helpful.

REFERENCES CITED

Aguillón-Robles, A., Calmus, T., Benoit, M., Bellon, H., Maury, R.C., Cotten, J., Bourgois, J., and Michaud, F., 2001, Late Miocene adakites and Nb-enriched basalts from Vizcaino Peninsula, Mexico: Indicators of East Pacific Rise subduction below southern Baja California?: Geology, v. 29, p. 531–534, https://doi.org/10.1130/0091-7613(2001)029<0531:LMAANE>2.0.CO;2.

Allen, P.A., and Allen, J.R., 2013, Basin Analysis: Principles and Application to Petroleum Play Assessment (third edition): Chichester, UK, Wiley-Blackwell, 632 p.

Andrews, G.D.M., Busby, C.J., Brown, S.R., McDowell, F., Fisher, C., Strickland, A., Vervoort, J.D., and Valley, J.W., 2012, Assessing Mantle versus Crustal Contributions to the Cenozoic Sierra Madre Occidental Silicic Large Igneous Province, Mexico: Insights from εHf and $\delta^{18}O$ in Zircon: San Francisco, American Geophysical Union Abstracts with Programs, abstract T21E-2618.

Angelier, J., Colletta, B., Chorowicz, J., Ortlieb, L., and Rangin, C., 1981, Fault tectonics of the Baja California peninsula and the opening of the Sea of Cortez: Journal of Structural Geology, v. 3, no. 4, p. 347–357, https://doi.org/10.1016/0191-8141(81)90035-3.

Atwater, T., 1970, Implications of plate tectonics for the Cenozoic tectonic evolution of Western North America: Geological Society of America Bulletin, v. 81, p. 3513–3536, https://doi.org/10.1130/0016-7606(1970)81[3513:IOPTFT]2.0.CO;2.

Atwater, T., 1989, Plate tectonic history of the northeast Pacific and western North America, *in* Winterer, E.L., Hussong, D.M., and Decker, R.W., eds., The Eastern Pacific Ocean and Hawaii: Boulder, Colorado, Geological Society of America, The Geology of North America, v. N, p. 21–72.

Atwater, T., and Stock, J., 1998, Pacific–North American plate tectonics of the Neogene southwestern United States: An update: International Geology Review, v. 40, p. 375–402, https://doi.org/10.1080/00206819809465216.

Axen, G., 1995, Extensional segmentation of the Main Gulf Escarpment, Mexico and United States: Geology, v. 23, p. 515–518, https://doi.org/10.1130/0091-7613(1995)023<0515:ESOTMG>2.3.CO;2.

Axen, G.J., and Fletcher, J.M., 1998, Late Miocene–Pleistocene extensional faulting, northern Gulf of California, Mexico and Salton Trough, California: International Geology Review, v. 40, p. 217–244, https://doi.org/10.1080/00206819809465207.

Axen, G.J., Grove, M., Stockli, D., Lovera, O.M., Rothstein, D.A., Fletcher, J.M., Farley, K., and Abbott, P.L., 2000, Thermal evolution of Monte Blanco dome: Low-angle normal faulting during Gulf of California rifting and late Eocene denudation of the eastern Peninsular Ranges: Tectonics, v. 19, p. 197–212, https://doi.org/10.1029/1999TC001123.

Balestrieri, M.L., Ferrari, L., Bonini, M., Duque-Trujillo, J., Cerca, M., Moratti, G., and Corti, G., 2017, Onshore and offshore apatite fission-track dating from the southern Gulf of California: Insights into the time-space evolution of the rifting: Tectonophysics, v. 719–720, p. 148–161, https://doi.org/10.1016/j.tecto.2017.05.012.

Bellon, H.V., Aguillón-Robles, A., Calmus, T., Maury, R.C., Bourgois, J., and Cotten, J., 2006, La Purísma volcanic field, Baja California Sur (Mexico): Miocene to Quaternary volcanism related to subduction and opening of an asthenospheric slab window: Journal of Volcanology and Geothermal Research, v. 152, p. 253–272, https://doi.org/10.1016/j.jvolgeores.2005.10.005.

Bennett, S.E.K., and Oskin, M.E., 2014, Oblique rifting ruptures continents: Example from the Gulf of California shear zone: Geology, v. 42, p. 215–218, https://doi.org/10.1130/G34904.1.

Bennett, S.E.K., Oskin, M.E., and Iriondo, A., 2013, Transtensional rifting in the proto-Gulf of California near Bahía Kino, Sonora, Mexico: Geological Society of America Bulletin, v. 125, p. 1752–1782, https://doi.org/10.1130/B30676.1.

Bennett, S.E.K., Oskin, M.E., Dorsey, R.J., Iriondo, A., and Kunk, M.J., 2015, Stratigraphy and structural development of the southwest Isla Tiburón marine basin: Implications for latest Miocene tectonic opening and flooding of the northern Gulf of California: Geosphere, v. 11, p. 977–1007, https://doi.org/10.1130/GES01153.1.

Bennett, S.E.K., Oskin, M.E., Iriondo, A., and Kunk, M.J., 2016, Slip history of the La Cruz fault: Development of a late Miocene transform in response to increased rift obliquity in the northern Gulf of California: Tectonophysics, v. 693, p. 409–435, https://doi.org/10.1016/j.tecto.2016.06.013.

Bennett, S.E.K., Oskin, M.E., and Iriondo, A., 2017, Latest Miocene transtensional rifting of northeast Isla Tiburón, eastern margin of the Gulf of California: Tectonophysics, v. 719–720, p. 86–106, https://doi.org/10.1016/j.tecto.2017.05.030.

Benoit, M., Aguillón-Robles, A., Calmus, T., Maury, R.C., Bellon, H., Cotten, J., Bourgois, J., and Michaud, F., 2002, Geochemical diversity of Late Miocene volcanism in southern Baja California, Mexico: Implication of mantle and crustal sources during the opening of an asthenospheric window: The Journal of Geology, v. 110, p. 627–648, https://doi.org/10.1086/342735.

Bonini, J.A., and Baldwin, S.L., 1998, Mesozoic metamorphic and middle to late Tertiary magmatic events on Magdalena and Santa Margarita Islands, Baja California Sur, Mexico: Implications for the tectonic evolution of the Baja California continental borderland: Geological Society of America Bulletin, v. 110, p. 1094–1104, https://doi.org/10.1130/0016-7606(1998)110<1094:MMAMTL>2.3.CO;2.

Bot, A., Geoffroy, L., Authemayou, C., Bellon, H., David, G., and Raphaël, P., 2016, Miocene detachment faulting predating EPR propagation, southern Baja California: Tectonics, v. 35, p. 1153–1176, https://doi.org/10.1002/2015TC004030.

Bouvier, A., Vervoort, J.D., and Pachett, P.J., 2008, The Lu-Hf and Sm-Nd isotopic composition of CHUR: Constraints from unequilibrated chondrites and implications for the bulk composition of terrestrial planets: Earth and Planetary Science Letters, v. 273, no. 1–2, p. 48–57, https://doi.org/10.1016/j.epsl.2008.06.010.

Branney, M.J., and Kokelaar, B.P., 1994, Volcanotectonic faulting, soft-sediment deformation, and rheomorphism of tuffs during development of a piecemeal caldera, English Lake District: Geological Society of America Bulletin, v. 106, no. 4, p. 507–530, https://doi.org/10.1130/0016-7606(1994)106<0507:VFSSDA>2.3.CO;2.

Busby, C.J., 2013, Birth of a plate boundary at ca. 12 Ma in the Ancestral Cascades arc, Walker Lane belt of California and Nevada: Geosphere, v. 9, p. 1147–1160, https://doi.org/10.1130/GES00928.1.

Busby, C.J., and Bassett, K., 2007, Volcanic facies architecture of an intra-arc strike-slip basin, Santa Rita Mountains, Arizona: Bulletin of Volcanology, v. 70, no. 1, p. 85–103, https://doi.org/10.1007/s00445-007-0122-9.

Busby, C.J., Bassett, K., Steiner, M.B., and Riggs, N.R., 2005, Climatic and tectonic controls on Jurassic intra-arc basins related to northward drift of North America, *in* Anderson, T.H., Nourse, J.A., McKee, J.W., and Steiner, M.B., eds., The Mojave-Sonora Megashear Hypothesis: Development, Assessment, and Alternatives: Geological Society of America Special Paper 393, p. 359–376, https://doi.org/10.1130/0-8137-2393-0.359.

Busby, C.J., Koerner, A., Melosh, B., Andrews, G., and Hagan, J., 2013a, Sierra Crest graben-vent system: A Walker Lane pull apart within the ancestral Cascades arc: Geosphere, v. 9, p. 736–780, https://doi.org/10.1130/GES00670.1.

Busby, C.J., Hagan, J., and Renne, P., 2013b, Initiation of Sierra Nevada range front—Walker Lane faulting at ca. 12 Ma in the ancestral Cascades arc: Geosphere, v. 9, p. 1–22, https://doi.org/10.1130/GES00927.1.

Busby, C.J., Andrews, G.D.M., Koerner, A.K., Brown, S.R., Melosh, B.L., and Hagan, J.C., 2016, Progressive derangement of ancient (Mesozoic) E-W Nevadaplano paleochannels into modern (Miocene–Recent) NNW trends in the Walker Lane belt, Central Sierra Nevada: Geosphere, v. 12, p. 135–175, https://doi.org/10.1130/GES01182.1.

Busby, C.J., Putirka, K., Melosh, B., Renne, P.R., Hagan, J.C., Gambs, M., and Wesoloski, C., 2018a, A tale of two Walker Lane Belt pull-apart basins in the Ancestral Cascades arc, central Sierra Nevada, California: Geosphere, v. 14, https://doi.org/10.1130/GES01398.1.

Busby, C.J., Graettinger, A., and López Martínez, M., 2018b, Volcano-tectonic evolution of the central Baja California Gulf margin: ^{40}Ar-^{39}Ar geochronological constraints: Geological Society of America Abstracts with Programs, v. 50, https://doi.org/10.1130/abs/2018RM-314304.

Calmus, T., Aguillón-Robles, A., Maury, R.C., Maury, R.C., Bellon, H., Benoit, M., Cotton, J., Bourgois, J., and Michaud, F., 2003, Spatial and temporal evolution of basalts and magnesian andesites ("bajaites") from Baja California, Mexico: The role of slab melts: Lithos, v. 66, p. 77–105, https://doi.org/10.1016/S0024-4937(02)00214-1.

Calmus, T., Pallares, C., Maury, R., Aguillón-Robles, A., Bellon, H., Benoit, M., and Michaud, F., 2011, Volcanic markers of the post-subduction evolution of Baja California and Sonora, Mexico: Slab tearing vs. lithospheric rupture of the Gulf of California: Pure and Applied Geophysics, v. 168, p. 1303–1330, https://doi.org/10.1007/s00024-010-0204-z.

Carlson, C.W., 2017, Kinematics and transfer mechanisms of strain accommodation at the transition between the northern and central Walker Lane, Western Nevada [unpublished dissertation]: University of Nevada Reno, 190 p.

Carlson, C.W., Pluhar, C.J., Glen, J.M.G., and Farner, M.J., 2013, Kinematics of the west-central Walker Lane: Spatially and temporally variable rotations evident in the Late Miocene Stanislaus Group: Geosphere, v. 9, no. 6, p. 1530–1551, https://doi.org/10.1130/GES00955.1.

Castillo, P.R., 2008, Origin of the adakite-high Nb basalt association and its implications for post-subduction magmatism in Baja California, Mexico: Geological Society of America Bulletin, v. 120, p. 451–462, https://doi.org/10.1130/B26166.1.

Castillo, P.R., 2012, Adakite petrogenesis: Lithos, v. 134–135, p. 304–316, https://doi.org/10.1016/j.lithos.2011.09.013.

Christie-Blick, N., and Biddle, K.T., 1985, Deformation and basin formation along strike-slip faults, *in* Christie-Blick, N., and Biddle, K.T., eds., Strike-Slip Deformation, Basin Formation, and Sedimentation: Society of Economic Paleontologists and Mineralogists Special Publication 37, p. 1–34, https://doi.org/10.2110/pec.85.37.0001.

Conly, A.G., Brenan, J.M., Bellon, H., and Scott, S.D., 2005, Arc to rift transitional volcanism in the Santa Rosalia region, Baja California Sur: Journal of Volcanology and Geothermal Research, v. 142, p. 303–341, https://doi.org/10.1016/j.jvolgeores.2004.11.013.

Conly, A.G., Beaudoin, G., and Scott, S.D., 2006, Isotopic constraints on fluid evolution and precipitation mechanisms for the Boléo Cu-Co-Zn deposit, Mexico: Mineralium Deposita, v. 41, p. 127–151, https://doi.org/10.1007/s00126-005-0045-3.

Conly, A.G., Scott, S.D., and Bellon, H., 2011, Metalliferous manganese oxide mineralization associated with the Boléo Cu-Co-Zn district: Economic Geology and the Bulletin of the Society of Economic Geologists, v. 106, p. 1173–1196, https://doi.org/10.2113/econgeo.106.7.1173.

Curray, J.R., Moore, D.G., and Shipboard Scientific Party, 1982, Guaymas basin: Sites 477, 478 and 481: Initial Reports of the Deep Sea Drilling Project, v. 64, p. 211–415, https://doi.org/10.2973/dsdp.proc.64.104.1982.

Darin, M.H., Bennett, S.E.K., Dorsey, R.J., Oskin, M.E., and Iriondo, A., 2016, Late Miocene extension in coastal Sonora, Mexico: Implications for the evolution of dextral shear in the proto-Gulf of California oblique rift: Tectonophysics, v. 693, p. 378–408, https://doi.org/10.1016/j.tecto.2016.04.038.

Delgado-Argote, L.A., López Martínez, M., and Perrilliat del Carmen, M., 2000, Geologic reconnaissance and Miocene age of volcanism and associated fauna from sediments of Bahía de Los Angeles, Baja California, central Gulf of California, *in* Delgado Granados, H., Aguirre Díaz, G.J., and Stock, J.M., eds., Cenozoic Tectonics and Volcanism of Mexico: Geological Society of America Special Paper 334, p. 111–121, https://doi.org/10.1130/0-8137-2334-5.111.

Di Luccio, F., Persaud, P., and Clayton, R.W., 2014, Seismic structure beneath the Gulf of California: A contribution from group velocity measurements: Geophysical Journal International, v. 199, no. 3, p. 1861–1877, https://doi.org/10.1093/gji/ggu338.

Dorsey, R.J., Umhoefer, P.J., and Renne, P., 1995, Rapid subsidence and stacked Gilbert-type fan deltas, Pliocene Loreto basin, Baja California Sur, Mexico: Sedimentary Geology, v. 98, p. 181–204, https://doi.org/10.1016/0037-0738(95)00032-4.

Drake, W.R., Umhoefer, P.J., Griffiths, A., Vlad, A., Peters, L., and McIntosh, W., 2017, Tectono-stratigraphic evolution of the Comondú Group from Bahia de La Paz to Loreto, Baja California Sur, Mexico: Tectonophysics, v. 719–720, p. 107–134, https://doi.org/10.1016/j.tecto.2017.04.020.

Duque-Trujillo, J., Ferrari, L., Orozco-Esquivel, T., López Martínez, M., Lonsdale, P., Bryan, S.E., Kluesner, J., Pinero-Lajas, D., and Solari, L., 2015, Timing of rifting in the southern Gulf of California and its conjugate margins: Insights from the plutonic record: Geological Society of America Bulletin, v. 127, no. 5/6, p. 702–736, https://doi.org/10.1130/B31008.1.

Escalona Alcazar, F.D.J., Delgado Argote, L.A., López Martínez, M., and Rendon Marquez, G., 2001, Late Miocene volcanism and marine incursions in the San Lorenzo Archipelago, Gulf of California, Mexico: Revista Mexicana de Ciencias Geológicas, v. 18, no. 2, p. 111–128.

Evans, R., 1978, Origin and significance of evaporates in basins around Atlantic margin: The American Association of Petroleum Geologists Bulletin, v. 62, p. 223–234.

Ferrari, L., Tagami, T., Eguchi, M., Orozco Esquivel, T., Petrone, C.M., Jacobo Albarrán, J., and López Martínez, M., 2005, Geology, geochronology and tectonic setting of late Cenozoic volcanism along the southwestern Gulf of Mexico: The Eastern Alkaline Province revisited: Journal of Volcanology and Geothermal Research, v. 146, p. 284–306, https://doi.org/10.1016/j.jvolgeores.2005.02.004.

Ferrari, L., Lopez-Martinez, M., Oroxco-Esquival, T., Bryan, S.E., Duque-Trujillo, J., Lonsdale, P., and Solari, L., 2013, Late Oligocene to Middle Miocene rifting and synextensional magmatism in the southwestern Sierra Madre Occidentale, Mexico: The beginning of the Gulf of California rift: Geosphere, v. 9, p. 1161–1200, https://doi.org/10.1130/GES00925.1.

Ferrari, L., Orozco-Esquivel, T., Bryan, S.E., López Martínez, M., and Silva-Fragoso, A., 2018, Cenozoic magmatism and extension in western Mexico: Linking the Sierra Madre Occidental silicic large igneous province and the Comondú Group with the Gulf of California rift: Earth-Science Reviews, v. 183, p. 115–152, https://doi.org/10.1016/j.earscirev.2017.04.006.

Fisher, R.V., and Schmincke, H.U., 1984, Pyroclastic Rocks: New York, Springer, 462 p., https://doi.org/10.1007/978-3-642-74864-6.

Fisher, R.V., Smith, A.L., and Roobol, M.J., 1980, Destruction of St Pierre, Martinique, by ash-cloud surge, May 8 and 20, 1902: Geology, v. 8, p. 472–476, https://doi.org/10.1130/0091-7613(1980)8<472:DOSPMB>2.0.CO;2.

Fletcher, J.M., Kohn, B.P., Foster, D.A., and Gleadow, A.J.W., 2000, Heterogeneous cooling and exhumation of the Los Cabos block, southern Baja California: Evidence from fission-track

thermochronology: Geology, v. 28, p. 107–110, https://doi.org/10.1130/0091-7613(2000)28<107:HNCAEO>2.0.CO;2.
Fletcher, J.M., Grove, M., Kimbrough, D., Lovera, O., and Gehrels, G.E., 2007, Ridge-trench interactions and the Neogene tectonic evolution of the Magdalena shelf and southern Gulf of California: Insights from detrital zircon ages from the Magdalena fan and adjacent areas: Geological Society of America Bulletin, v. 119, no. 11/12, p. 1313–1336, https://doi.org/10.1130/B26067.1.
Freundt, A., Wilson, C.J.N., and Carey, S.N., 2000, Ignimbrites and block-and-ash flow deposits, *in* Sigurdsson, H., Houghton, B.F., McNutt, S.R., Rymer, H., and Stix, J., eds., Encyclopedia of Volcanoes: New York, Academic Press, p. 581–600.
García-Sánchez, L., Luis Macías, J., Osorio-Ocampo, S., Sosa-Ceballos, G., Pola, A., Ramón Avellán, D., Luis Arce, J., Saucedo, R., García, F., Reyes-Agustín, G., Cardona, S., and Cisneros, G., 2016, Volcanic and magmatic evolution of Reforma Caldera, BCS, Mexico: Puerta Varas, IAVCEI Cities on Volcanoes abstract, November 20–25.
Gastil, G., Krummenacher, D., and Minch, J., 1979, The record of Cenozoic volcanism around the Gulf of California: Geological Society of America Bulletin, v. 90, p. 839–857, https://doi.org/10.1130/0016-7606(1979)90<839:TROCVA>2.0.CO;2.
Harris, A.C., Kamenetsky, V.S., White, N.C., and Steele, D.A., 2004, Volatile phase separation in silicic magmas at Bajo de la Alumbrera porphyry Cu-Au deposit, NW Argentina: Resource Geology, v. 54, no. 3, p. 341–356, https://doi.org/10.1111/j.1751-3928.2004.tb00210.x.
Hausback, B.P., 1984, Cenozoic volcanic and tectonic evolution of Baja California, Mexico, *in* Frizzell, V.A., ed., Geology of the Baja California Peninsula: Pacific Section, Society of Economic Paleontologists and Mineralogists, Bakersfield, California, p. 219–236.
Henry, C.D., and Aranda-Gomez, J.J., 2000, Plate interactions control middle-late Miocene proto-Gulf and Basin and Range extension in the southern Basin and Range: Tectonophysics, v. 318, p. 1–26, https://doi.org/10.1016/S0040-1951(99)00304-2.
Henry, M., 2019, Detrital zircon geochronology of the Upper Miocene Boleo Formation in the Santa Rosalía basin, Baja California Sur, Mexico [M.S. thesis]: University of Missouri, Kansas City, 104 p.
Henry, M., Harrison, D.M., Martínez-Gutierrez, G., Murowchick, J.B., Lee, J., and Niemi, T.M., 2015, Distribution and depositional model of the Cinta Colorada marker bed of the copper-rich Boleo Formation, Santa Rosalía basin, Baja California Sur, Mexico: Geological Society of America Abstracts with Program, v. 47, no. 7, p. 541.
Henry, M., Alvarez Ortega, K.G., Banes, A., Holm-Denoma, C., Busby, C., and Niemi, T.M., 2017, Detrital zircon U-Pb geochronology of the Boleo Formation of Santa Rosalía basin, Baja California Sur, Mexico: American Geophysical Union Meeting, New Orleans, Louisiana, December 11–15, 2017.
Holt, J.W., Holt, E.W., and Stock, J.M., 2000, An age constraint on Gulf of California rifting from the Santa Rosalía basin, Baja California Sur, Mexico: Geological Society of America Bulletin, v. 112, p. 540–549, https://doi.org/10.1130/0016-7606(2000)112<540:AACOGO>2.0.CO;2.
Hopper, J.R., and Buck, W.R., 1996, The effect of lower crustal flow on continental extension and passive margin formation: Journal of Geophysical Research, v. 101, p. 20175–20194, https://doi.org/10.1029/96JB01644.
Ingersoll, R.V., and Busby, C.J., 1995, Tectonics of Sedimentary Basins: Oxford, UK, Blackwell Science, p. 1–51.
Jackson, M., and Cramez, C., 2000, Role of subaerial volcanic rocks and mantle plumes in creation of South Atlantic margins: Implications for salt tectonics and source rocks: Marine and Petroleum Geology, v. 17, p. 477–498, https://doi.org/10.1016/S0264-8172(00)00006-4.
Kiddle, E.J., Edwards, B.R., Loughlin, S.C., Petterson, M., Sparks, R.S.J., and Voight, B., 2010, Crustal structure beneath Montserrat, Lesser Antilles, constrained by xenoliths, seismic velocity structure and petrology: Geophysical Research Letters, v. 37, L00E11, https://doi.org/10.1029/2009GL042145.
Lambert, M.B., 1974, The Bennett Lake cauldron subsidence complex, British Columbia and Yukon Territory: Geological Survey of Canada Bulletin 227, 213 p, https://doi.org/10.4095/103475.
Lee, J., Miller, M.M., Crippen, R., Hacker, B., and Vazquez, J.L., 1996, Middle Miocene extension in the Gulf Extensional Province, Baja California: Evidence from the southern Sierra Juarez: Geological Society of America Bulletin, v. 108, p. 505–525, https://doi.org/10.1130/0016-7606(1996)108<0505:MMEITG>2.3.CO;2.
Lipman, P.W., 1976, Caldera-collapse breccias in the western San Juan Mountains, Colorado: Geological Society of America Bulletin, v. 87, no. 10, p. 1397–1410, https://doi.org/10.1130/0016-7606(1976)87<1397:CBITWS>2.0.CO;2.
Lizarralde, D., Axen, G.J., Brown, H.E., Fletcher, J., Gonzáles-Fernández, A., Harding, A.J., Holbrook, W.S., Kent, G.M., Paramo, P., Sutherland, F., and Umhoefer, P.J., 2007, Variation in styles of rifting in the Gulf of California: Nature, v. 448, p. 466–469, https://doi.org/10.1038/nature06035.
Lonsdale, P., 1991, Structural patterns of the Pacific floor offshore of peninsular California, *in* Dauphin, J.P., and Simoneit, B.R.T., eds., The Gulf and Peninsular Province of the Californias: American Association of Petroleum Geologists Memoir, v. 47, p. 87–125.
Martín-Barajas, A., Stock, J.M., Layer, P., Hausback, B., Renne, P.M., and López-Martínez, M., 1995, Arc-rift transition volcanism in the Puertecitos Volcanic Province, northeastern Baja California, Mexico: Geological Society of America Bulletin, v. 107, no. 4, p. 407–424, https://doi.org/10.1130/0016-7606(1995)107<0407:ARTVIT>2.3.CO;2.
Martín-Barajas, A., Tellez-Duarte, M., and Stock, J.M., 1997, The Puertecitos Formation: Pliocene volcaniclastic sedimentation along an accommodation zone in northeastern Baja California, *in* Johnson, M.E., and Ledesma-Vazquez, J., eds., Pliocene Carbonate and Related Facies Flanking the Gulf of California, Baja California, Mexico: Geological Society of America Special Paper 318, p. 1–24, https://doi.org/10.1130/0-8137-2318-3.1.
Martín-Barajas, A., Fletcher, J., López Martínez, M., and Mendoza Borunda, R., 2000, Waning Miocene subduction and arc volcanism in Baja California: The San Luis Gonzaga volcanic field, *in* Ferrari, L., Stock, J.M., and Urrutia Fucugauchi, J., eds., Post-Laramide Magmatism and Tectonics in Mexico and Plate Interactions: Tectonophysics, v. 318, p. 27–51.
Martín-Barajas, A., González-Escobar, M., Fletcher, J.M., Pacheco, M., Oskin, M., and Dorsey, R., 2013, Thick deltaic sedimentation and detachment faulting delay the onset of continental rupture in the Northern Gulf of California: Analysis of seismic profiles: Tectonics, v. 32, p. 1294–1311, https://doi.org/10.1002/tect.20063.
McCann, K.A., Dorsey, R.J., Niemi, T.M., and Jaime-Geraldo, A.J., 2017, Stratigraphic analysis of the Late Miocene Boleo Formation, Santa Rosalia Basin Baja California Sur, Mexico: Geological Society of America Abstracts with Programs, v. 49, no. 6, https://doi.org/10.1130/abs/2017AM-308157.
McCurry, M., and Schmidt, K., 2001, Petrology and oxygen isotope geochemistry of the Pucon Ignimbrite–Southern Andean Volcanic Zone, Chile: Implications for genesis of mafic ignimbrites: Santiago, Chile, III South American Symposium Isotope Geology, Geological Society of Chile, p. 317–320.
McLean, H., Hausback, B.P., and Knapp, J.H., 1987, The geology of west-central Baja California Sur, Mexico: U.S. Geological Survey Bulletin 1579, p. 1–16.
Michaud, F., Sosson, M., Royer, J.-Y., Chabert, A., Bourgois, J., Calmus, T., Mortera, C., Bandy, W., Dyment, J., Pontoise, B., and Sichler, B., 2004, Motion partitioning between the Pacific plate, Baja California and the North America plate: The Tosco-Abreojos fault revisited: Geophysical Research Letters, v. 31, https://doi.org/10.1029/2004GL019665.
Michaud, F., Royer, J.Y., Bourgois, J., Dyment, J., Calmus, T., Bandy, W., Sosson, M., Mortera-Gutiérrez, C., Sichler, B., Rebolledo-Viera, M., and Pontoise, B., 2006, Oceanic-ridge subduction vs. slab break off: Plate tectonic evolution along the Baja California Sur continental margin since 15 Ma: Geology, v. 34, no. 1, p. 13–16, https://doi.org/10.1130/g22050.1.
Miller, N.C., and Lizarralde, D., 2013, Thick evaporates and early rifting in the Guaymas basin, Gulf of California: Geology, v. 41, p. 283–286, https://doi.org/10.1130/G33747.1.
Moyen, J.-P., 2009, High Sr/Y and La/Yb ratios: The meaning of the “adakitic signature”: Lithos, v. 112, p. 556–574, https://doi.org/10.1016/j.lithos.2009.04.001.
Murray, B., Busby, C.J., Ferrari, L., and Solari, L.A., 2013, Synvolcanic crustal extension during the mid-Cenozoic ignimbrite flare-up in the northern Sierra Madre Occidental, Mexico: Evidence from the Guazapares Mining District region, western Chihuahua: Geosphere, v. 9, https://doi.org/10.1130/GES00862.1.
Nagy, E.A., Grove, M., and Stock, J.M., 1999, Age and stratigraphic relationships of pre- and syn-rift volcanic deposits in the northern Puertecitos Volcanic Province, Baja California, Mexico: Journal of Volcanology and Geothermal Research, v. 93, p. 1–30, https://doi.org/10.1016/S0377-0273(99)00080-3.
Negrete-Aranda, R., and Cañón-Tapia, E., 2008, Post-subduction volcanism in the Baja California Peninsula, Mexico: The effects of tectonic reconfiguration in volcanic systems: Lithos, v. 102, p. 392–414, https://doi.org/10.1016/j.lithos.2007.08.013.
Negrete-Aranda, R., Cañón-Tapia, E., Brandle, J.L., Ortega-Rivera, M.A., Lee, J.K.W., Spelz, R.M., and Hinojosa-Corona, A., 2010, Regional orientation of tectonic stress and the stress expressed by post-subduction high-magnesium volcanism in northern Baja California Peninsula, Mexico: Tectonics and volcanism of San Borja volcanic field: Journal of Volcanology and Geothermal Research, v. 192, p. 97–115, https://doi.org/10.1016/j.jvolgeores.2010.02.014.
Negrete-Aranda, R., Contreras, J., and Spelz, R.M., 2013, Viscous dissipation, slab melting, and post-subduction volcanism

in the south-central Baja California: Geosphere, v. 9, https://doi.org/10.1130/GES00901.1.

Nilsen, T.H., and McLaughlin, R.J., 1985, Comparison of tectonic framework and depositional patterns of the Hornelen strike-slip basin of Norway and the Ridge and Little Sulfur Creek strike-slip basins of California, *in* Biddle, N.T., and Christie-Blick, N., eds., Strike-Slip Deformation, Basin Formation and Sedimentation: Society for Sedimentary Geology, v. 37, p. 79–103, https://doi.org/10.2110/pec.85.37.0079.

Nilsen, T.H., and Sylvester, A.G., 1995, Strike–slip basins, *in* Busby, C., and Ingersoll, R., eds., Tectonics of Sedimentary Basins: Oxford, Blackwell Science, p. 425–456.

Ochoa-Landín, L., Ruíz, J., Calmus, T., Perez-Segura, E., and Escandon, F., 2000, Sedimentology and stratigraphy of the Upper Miocene El Boleo Fm., Santa Rosalia, Baja California, Mexico: Revista Mexicana de Ciencias Geológicas, v. 17, p. 83–96.

Orszag-Sperber, F., Harwood, G., Kendall, A., and Purser, B.H., 1998, A review of the evaporates of the Red Sea–Gulf of Suez rift, *in* Purser, B.H., and Bosence, D.W., eds., Sedimentation and Tectonics in Rift Basins: Red Sea–Gulf of Aden: London, Chapman and Hall, p. 409–426.

Ortlieb, L., and Colletta, B., 1984, Síntesis cronoestratigrafica sobre el Neogeno y el Cuaternario marino de la cuenca Santa Rosalía, Baja California Sur, Mexico, *in* Malpica-Cruz, V., ed., Neotectonics and Sea Level Variations in the Gulf of California Area, A Symposium: Universidad Nacional Autónoma de México, Instituto de Geologica Revista, v. 8, p. 241–260.

Oskin, M., and Stock, J.M., 2003a, Pacific-North America plate motion and opening of the Upper Delfín basin, northern Gulf of California: Geological Society of America Bulletin, v. 115, p. 1173–1190, https://doi.org/10.1130/B25154.1.

Oskin, M., and Stock, J.M., 2003b, Marine incursion synchronous with plate-boundary localization in the Gulf of California: Geology, v. 31, p. 23–26, https://doi.org/10.1130/0091-7613(2003)031<0023:MISWPB>2.0.CO;2.

Oskin, M., and Stock, J.M., 2003c, Cenozoic volcanism and tectonics of the continental margins of the Upper Delfín basin, northeastern Baja California and western Sonora, *in* Kimbrough, D.L., Johnson, S.E., Paterson, S., Martín-Barajas, A., Fletcher, J.M., and Girty, G., eds., Tectonic Evolution of Northwestern Mexico and the Southwestern USA: Geological Society of America Special Paper 374, p. 421–428, https://doi.org/10.1130/0-8137-2374-4.421.

Oskin, M., Stock, J., and Martín-Barajas, A., 2001, Rapid localization of Pacific–North America plate motion in the Gulf of California: Geology, v. 29, p. 459–462, https://doi.org/10.1130/0091-7613(2001)029<0459:RLOPNA>2.0.CO;2.

Osorio-Ocampo, S., Luis Macías, J.L., Garcia-Sánchez, L., Sosa Ceballos, G., Pola-Villaseñor, A., and García-Tenorio, F., 2016, Calc-alkaline magmatism of El Aguajito caldera, Baja California Sur, México: Puerta Varas, IAVCEI Cities on Volcanoes abstract, November 20–25.

Pallares, C., Maury, R.C., Bellon, H., Royer, J.-Y., Calmus, T., Aguillón-Robles, A., Cotten, J., Benoit, M., Michaud, F., and Bourgois, J., 2007, Slab-tearing following ridge-trench collision: Evidence from Miocene volcanism in Baja California, Mexico: Journal of Volcanology and Geothermal Research, v. 161, p. 95–117, https://doi.org/10.1016/j.jvolgeores.2006.11.002.

Pallares, C., Bellon, H., Benoit, M., Maury, R.C., Aguillón-Robles, A., Calmus, T., and Cotten, J., 2008, Slab-tearing following ridge-trench collision: Evidence from Miocene volcanism in Baja California, Mexico: Lithos, v. 105, p. 162–180, https://doi.org/10.1016/j.lithos.2008.03.004.

Paz Moreno, F.A.P., and Demant, A., 1999, The Recent Isla San Luis volcanic center: Petrology of a rift-related volcanic suite in the northern Gulf of California, Mexico: Journal of Volcanology and Geothermal Research, v. 93, p. 31–52, https://doi.org/10.1016/S0377-0273(99)00083-9.

Pitman, W.C., III, and Andrews, J.A., 1985, Subsidence and thermal history of small pull-apart basins, *in* Biddle, K.T., and Christie-Blick, N., eds., Strike-Slip Deformation, Basin Formation, and Sedimentation: Society of Economic Paleontologists and Mineralogists Special Publication 37, p. 45–119.

Putirka, K., and Busby, C.J., 2007, The tectonic significance of high K$_2$O volcanism in the Sierra Nevada, California: Geology, v. 35, p. 923–926, https://doi.org/10.1130/G23914A.1.

Putirka, K., and Platt, B., 2012, Basin and Range volcanism as a passive response to extensional tectonics: Geosphere, v. 8, p. 1274–1285, https://doi.org/10.1130/GES00803.1.

Putirka, K., Jean, M., Sharma, R., Torrez, G., and Carlson, C., 2012, Cenozoic volcanism in the Sierra Nevada, and a new model for lithosphere degradation: Geosphere, v. 8, p. 265–291, https://doi.org/10.1130/GES00728.1.

Richards, J.P., and Kerrich, R., 2007, Special Paper: Adakite-like rocks: Their diverse origins and questionable role in metallogenesis: Bulletin of the Society of Economic Geologists, v. 102, p. 537–576, https://doi.org/10.2113/gsecongeo.102.4.537.

Rogers, G., and Saunders, A.D., 1989, Magnesian andesites from Mexico, Chile and the Aleutian Islands: Implications for magmatism associated with ridge-trench collision, *in* Crawford, A.J., ed., Boninites: London, UK, Unwin Hyman, p. 416–445.

Rossi, M.W., Quigley, M.C., Fletcher, J.M., Whipple, K.X., Jesús Díaz-Torres, J., Seller, C., Fifield, K., and Heimsath, A.J., 2017, Along-strike variation in catchment morphology and cosmogenic denudation rates reveal the pattern and history of footwall uplift, Main Gulf Escarpment, Baja California: Geological Society of America Bulletin, v. 129, no. 7/8, p. 837–854, https://doi.org/10.1130/B31373.1.

Sato, H., Holtz, F., Behrens, H., Botcharnikov, R., and Nakada, S., 2005, Experimental petrology of the 1991–1995 Unzen dacite, Japan: Cl/OH partitioning between hornblende and melt and its implications for the origin of oscillatory zoning of hornblende phenocrysts: Journal of Petrology, v. 46, no. 2, p. 339–354, https://doi.org/10.1093/petrology/egh078.

Sawlan, M.G., 1991, Magmatic evolution of the Gulf of California rift, *in* Dauphin, J.P., and Simoneit, B.R., eds., The Gulf and Peninsular Province of the California: American Association of Petroleum Geologists Memoir 47, p. 301–369.

Sawlan, M.G., and Smith, J.G., 1984, Petrologic characteristics, age and tectonic setting of Neogene volcanic rocks in northern Baja California Sur, Mexico, *in* Frizzell, V.A., Jr., ed., Geology of the Baja California Peninsula, Pacific Section Society of Economic Paleontologists and Mineralogists, v. 39, p. 237–251.

Schermer, E.R., and Busby, C.J., 1994, Jurassic magmatism in the central Mojave Desert: Implications for arc paleogeography and preservation of continental volcanic sequences: Geological Society of America Bulletin, v. 106, p. 767–790, https://doi.org/10.1130/0016-7606(1994)106<0767:JMITCM>2.3.CO;2.

Schmidt, E.K., 1975, Plate tectonics, volcanic petrology, and ore formation in the Santa Rosalía area, Baja California, Mexico [M.S. thesis]: Phoenix, University of Arizona, Department of Geosciences, 187 p.

Schmitt, A.K., Stockli, D.F., and Hausback, B.P., 2006, Eruption and magma crystallization ages of Las Tres Vírgenes (Baja California) constrained by combined ^{230}Th/^{238}U and (U-Th)/He dating of zircon: Journal of Volcanology and Geothermal Research, v. 158, p. 281–295, https://doi.org/10.1016/j.jvolgeores.2006.07.005.

Schmitt, A.K., Stockli, D.F., Niedermann, S., Lovera, O.M., and Hausback, B.P., 2010, Eruption ages of the Las Tres Vírgenes volcano (Baja California): A tale of two helium isotopes: Quaternary Geochronology, v. 5, p. 503–511, https://doi.org/10.1016/j.quageo.2010.02.004.

Schmitt, A.K., Martín-Barajas, A., Weber, B., Stockli, D.F., Zou, H., and Shen, C.C., 2013, Oceanic magmatism in sedimentary basins of the northern Gulf of California rift: Geological Society of America Bulletin, v. 125, p. 1833–1850, https://doi.org/10.1130/B30787.1.

Seiler, C., Fletcher, J.M., Kohn, B.P., Gleadow, A.J.W., and Raza, A., 2011, Low-temperature thermochronology of northern Baja California, Mexico: Decoupled slip-exhumation gradients and delayed onset of oblique rifting across the Gulf of California: Tectonics, v. 30, TC3004, https://doi.org/10.1029/2009TC002649.

Seiler, C., Quigley, M.C., Fletcher, J.M., Phillips, D., Gleadow, A.J.W., and Kohn, B.P., 2013, Stratigraphy and ^{40}Ar-^{39}Ar geochronology of the Santa Rosa basin, Baja California: Dynamic evolution of a constrictional rift basin during oblique extension in the Gulf of California: Basin Research, v. 25, p. 388–418, https://doi.org/10.1111/bre.12004.

Sosa-Ceballos, G., Macías, J.L., Avellán, J.L., Arce, R., Saucedo, M., Boijseaneau-López, L., García-Sanchez, G., Reyes-Agustine, S., and Osorio-Ocampo, S., 2019, Genesis of magmas from the Tres Vírgenes volcanic complex, Baja California Sur, Mexico: Lithos, v. 350–351, https://doi.org/10.1016/j.lithos.2019.105240.

Sparks, R.S.J., 1997, Causes and consequences of pressurization in lava dome eruptions: Earth and Planetary Science Letters, v. 150, p. 177–189, https://doi.org/10.1016/S0012-821X(97)00109-X.

Stock, J.M., 2000, Relation of the Puertecitos Volcanic Province, Baja California, Mexico, to development of the plate boundary in the Gulf of California, *in* Delgado-Granados, H., Aguirre-Díaz, G., and Stock, J.M., eds., Cenozoic Tectonics and Volcanism of Mexico: Geological Society of America Special Paper 334, p. 143–156, https://doi.org/10.1130/0-8137-2334-5.143.

Stock, J.M., and Hodges, K.V., 1989, Pre-Pliocene extension around the Gulf of California and the transfer of Baja California to the Pacific plate: Tectonics, v. 8, p. 99–115, https://doi.org/10.1029/TC008i001p00099.

Stock, J.M., and Hodges, K.V., 1990, Miocene to Recent structural development of an extensional accommodation zone, northeastern Baja California, Mexico: Journal of Structural Geology, v. 12, p. 315–328, https://doi.org/10.1016/0191-8141(90)90016-R.

Stock, J.M., Lewis, C.J., and Nagy, E.A., 1999, The Tuff of San Felipe; an extensive middle Miocene pyroclastic flow deposit in Baja California, Mexico: Journal of Volcanology and Geothermal Research, v. 93, no. 1–2, p. 53–74, https://doi.org/10.1016/S0377-0273(99)00079-7.

Sun, S.-s., and McDonough, W.F., 1989, Chemical and isotopic systematics of oceanic basalts: Implications for mantle composition and processes, *in* Saunders, D., and Norry, M.J., eds., Magmatism in the Ocean Basins: Geological Society of London Special Publication 42, p. 313–345, https://doi.org/10.1144/GSL.SP.1989.042.01.19.

Sutherland, F.H., Kent, G.M., Harding, A.J., Umhoefer, P.J., Driscoll, N.W., Lizarralde, D., Fletcher, J.M., Axen, G.J., Holbrook, W.S., Gonzalez-Fernandez, A., and Lonsdale, P., 2012, Middle Miocene to early Pliocene oblique extension in the southern Gulf of California: Geosphere, v. 8, p. 752–770, https://doi.org/10.1130/GES00770.1.

Teske, A., Lizarralde, D., and Höfig, T.W., 2018, Expedition 385 Scientific Prospectus: Guaymas Basin Tectonics and Biosphere: International Ocean Discovery Program, https://doi.org/10.14379/iodp.sp.385.2018.

Till, C.B., Gans, P.B., Spera, F.J., Macmillon, I., and Blair, K.D., 2009, Perils of petrotectonic modeling: A view from southern Sonora, Mexico: Journal of Volcanology and Geothermal Research, v. 186, p. 160–168, https://doi.org/10.1016/j.jvolgeores.2009.06.014.

Umhoefer, P.J., 2011, Why did the southern Gulf of California rupture so rapidly?—Oblique divergence across hot, weak lithosphere along a tectonically active margin: GSA Today, v. 21, no. 11, p. 4–10, https://doi.org/10.1130/G133A.1.

Umhoefer, P.J., Dorsey, R.J., Willsey, S., Mayer, L., and Renne, P., 2001, Stratigraphy and geochronology of the Comondú Group near Loreto, Baja California Sur, Mexico: Sedimentary Geology, v. 144, p. 125–147, https://doi.org/10.1016/S0037-0738(01)00138-5.

Umhoefer, P.J., Darin, M.H., Bennett, S.E.K., Skinner, L.A., Dorsey, R.J., and Oskin, M.E., 2018, Breaching of strike-slip faults and successive flooding of pull-apart basins to form the Gulf of California seaway from ca. 8–6 Ma: Geology, v. 46, p. 695–698, https://doi.org/10.1130/G40242.1.

Walker, G.P.L., and Wilson, C.J.N., 1983, Lateral variations in the Taupo ignimbrite: Journal of Volcanology and Geothermal Research, v. 18, p. 117–133, https://doi.org/10.1016/0377-0273(83)90005-7.

Wang, Y., Forsyth, D.W., Rau, C.J., Carriero, N., Schmandt, B., Gaherty, J.B., and Savage, B., 2013, Fossil slabs attached to unsubducted fragments of the Farallon plate: Proceedings of the National Academy of Sciences of the United States of America, v. 110, p. 5342–5346, https://doi.org/10.1073/pnas.1214880110.

Wilson, I.F., and Rocha, V.S., 1955, Geology and Mineral Deposits of the Boleo Copper District, Baja California, Mexico: U.S. Geological Survey Professional Paper 273, 134 p., https://doi.org/10.3133/pp273.

Xie, X., and Heller, P.L., 2009, Plate tectonics and basin subsidence history: Geological Society of America Bulletin, v. 121, p. 55–64, https://doi.org/10.1130/B26398.1.